NACA RM E54B25

NACA

RESEARCH MEMORANDUM

INVESTIGATION OF IMPULSE-TYPE SUPERSONIC COMPRESSOR WITH HUB-TIP RATIO OF 0.6 AND TURNING TO AXIAL DIRECTION

I - PERFORMANCE OF ROTOR ALONE

By Ward W. Wilcox

Lewis Flight Propulsion Laboratory
Cleveland, Ohio

NATIONAL ADVISORY COMMITTEE
FOR AERONAUTICS

WASHINGTON

May 6, 1954

NACA RM E54B25

NATIONAL ADVISORY COMMITTEE FOR AERONAUTICS

RESEARCH MEMORANDUM

INVESTIGATION OF IMPULSE-TYPE SUPERSONIC COMPRESSOR WITH HUB-TIP RATIO OF 0.6 AND TURNING TO AXIAL DIRECTION

I - PERFORMANCE OF ROTOR ALONE

By Ward W. Wilcox

SUMMARY

The supersonic-compressor rotor described herein was designed as an impulse type with some deceleration along the tip and with turning to the axial direction. Design speed was 1400 feet per second, and the rotor was stressed to operate in air. Guide vanes were provided to set up a 16° counter-prerotation at the tip with free-vortex-type distribution radially. Tests of the rotor and guide vanes determined that, at design speed, the maximum pressure ratio of 4.7 and peak efficiency of 0.85 occurred at the maximum weight flow of 24.84 pounds per second per square foot of frontal area. At this operating point, the average outlet Mach number was 1.75 and the average flow angle was 43.5°. At 90 percent speed, flow conditions were judged to be more satisfactory for stator work, inasmuch as the average Mach number dropped to 1.4 at a flow angle of 47°. At this point, the pressure ratio was 3.7, efficiency 0.86, and the weight flow 23.6 pounds per second per square foot of frontal area. The radial distributions of pressure ratio, Mach number, and flow angle were considered satisfactory at this speed.

INTRODUCTION

Analysis (ref. 1) of the various possible arrangements utilizing supersonic flow in compressors has indicated several promising design configurations. For pressure ratios in the range from 3 to 7 the impulse, or shock-free, compressor was found to be most promising, and accordingly three such rotors were designed and tested in Freon-12. The first, for lower pressure ratios, discharged the gas in a direction approximately 10° less than axial and is reported in reference 2. For much higher pressure ratios, the same rotor was fitted with blades which turned about 10° past axial. The performance of this configuration is given in reference 3. In the middle range of pressure ratio, an impulse rotor was designed and tested (ref. 4) which turned the air exactly to the axial direction at all radii. The design tip speed of each of these rotors was 1600 feet per second.

During performance tests of the latter rotor, it was found that a shock could be stabilized in the rotor, thereby decreasing appreciably the outlet Mach number. This decrease in Mach number was obtained without an apparent sacrifice in adiabatic efficiency, and in fact, the best performance of this rotor was obtained at speeds lower than design without impulse operation.

On the basis of the performance of these three rotors, it was concluded that useful single-stage supersonic-compressor rotors could be designed with satisfactory rotor adiabatic efficiency. However, the stage efficiency, to date, has been relatively poor as a result of either high losses in the stator or poor matching of rotor and stator (ref. 5). The need for detailed diffuser studies is an obvious requirement before good stage performance can be expected.

The rotor reported herein was made specifically to aid in the stator investigations. This rotor was designed for more uniform outlet-flow conditions at a higher mass-flow rate and was stressed for operation in air. Design weight flow was 25.6 pounds per second per square foot of frontal area and design tip speed was 1400 feet per second.

In order to provide a basis for comparison of over-all performance with the various stators installed, the rotor performance was determined over a range of tip speed and weight flow with the inlet guide vanes at their design setting. In addition, surveys of outlet-flow conditions were obtained at all test points to facilitate the design of diffusing stators. The results of the rotor performance tests are reported herein.

ROTOR DESIGN

The rotor tip speed was selected at 1400 feet per second. The reduction in design speed from the 1600 feet per second of references 2 to 4 was a result of consideration of the effect of the increase in the flow capacity on the stress level of both the turbine and compressor (ref. 6). In order to compensate for the reduction in rotor speed and to reduce the radial gradient of work input, a prewhirl of 16° at the tip with free-vortex distribution to 25.6° at the hub-radius ratio of 0.6 was imparted counter to the direction of rotation. Design turning in the rotor was to the axial direction at all radii. The design method was basically a modified stream-filament method and follows very closely that reported in reference 4. The rotor was designed for a nearly constant relative velocity at the entrance and exit mean diameters. Because of the increased static pressure resulting from the change in radius of the mean streamline and the increased static-pressure gradient due to the high-whirl component at the rotor discharge, the tip streamline required an appreciable static-pressure rise across the rotor. The prescribed tip mean-velocity ratio

Q varied from 1.573 at the entrance to 1.354 at the exit, with the variation along the rotor axis shown in figure 1. A slight acceleration was allowed near the entrance in an effort to avoid deceleration to subsonic relative velocities along the rotor hub. The prescribed relative mean flow direction at the tip is shown in figure 2, plotted as the tangent of the angle against distance along the rotor axis. The prescribed thickness distribution for the computed blade shape is shown in figure 3. By altering the suction surface of the computed blade, an arbitrary boundary-layer and loss allowance was made. This allowance varied linearly from zero at the entrance to 10 percent of the passage width at the blade exit. A blade mean surface was formed by extending radial elements through the tip mean line. At each axial position, the untapered blades were symmetrical about this mean surface. The streamlines through the rotor and a layout of the real and computed blade shapes are shown in figure 4. The sweepback of the leading edge was required to match the flow entrance angles along the radius. The section forward of the tip leading edge had a constant thickness of 0.050 inch. By using 29 rotor blades, the rotor diffusion, defined as $(V'_{max} - V'_{min})/V'_e$ (ref. 7), was held to approximately 0.3. (All symbols are defined in the appendix.)

The isentropic pressure ratio for this design ranged from 6.9 at the tip to 4.1 at the hub at an equivalent weight flow of 25.6 pounds per second per square foot of frontal area (with no boundary-layer allowance at the inlet). The rotor, which was 16 inches in diameter and 5.19 inches in length, is shown in figure 5. Fabrication was by milling from a 14S-T6 aluminum forging.

Coordinates of the blade, leading edge, and hub are given in table I.

To avoid choking in the guide vanes, the hub-radius ratio was reduced to 0.5 at their location 5.13 inches upstream of the rotor. The 23 circular-arc sheet-metal guide vanes were designed according to the turning rule of reference 8 and corrected for end effects according to reference 9. In order to improve the solidity at the tip, the radius of curvature was reduced uniformly with decreasing radius. For this reason, the resulting blade was a section of the surface of a cone. Desired air-discharge angles were then established by control of the arc length at each radius. The photograph of figure 6 shows the guide-vane installation.

APPARATUS

Test rig. - As shown in figure 7, the rotor was installed in the standard 16-inch variable-component compressor test rig described in reference 2. The compressor was driven by a 3000-horsepower variable-frequency motor. Air flow was regulated by butterfly valves in the inlet and outlet ducting, and in addition a throttle built into the collector (fig. 7) was used to control back pressure.

Instrumentation. - Room-temperature air was measured by an open-end orifice and the refrigerated air by an adjustable Bailey meter. Nearly all measured weight flows agreed with integrated values from the surveys within ±3 percent. In figure 7, the locations of the measuring stations are given, and the following instruments, some of which are illustrated in figure 8, were used as follows:

Station 1 (plenum tank) - six shielded total-pressure tubes, six static taps, six bare-wire thermocouples

Station 2 (behind guide vanes) - 19-tube total-pressure rake, miniature claw for angle and total pressure, seven wall statics

Station 3 (1 in. in front of rotor at tip) - miniature claw, four statics

Station 5 (1 in. behind rotor) - miniature claw, split-shield thermocouple, L-static probe, 16 static taps.

In addition, 21 static taps were placed at 1/4-inch axial spacing on the casing over the rotor, and others were spaced at intervals along the axis. Static pressures were led to well-type manometers, photographed, and then processed in IBM equipment to obtain absolute static pressure. All temperatures were read on a calibrated self-balancing potentiometer. Each individual thermocouple was calibrated for Mach number and density effects in a separate wind tunnel. In addition, the recovery of each miniature claw and the calibration of each static probe was determined over the range of Mach number encountered.

3219

OPERATING PROCEDURE

With all outlet throttles open, the desired tip speed and inlet tank pressure were established. The outlet claw probe was set at midstream, other probes drawn to the wall position, and a photograph of the static pressures taken. Individual surveys were made with one instrument at a time to minimize blockage effects. Seven radial survey positions were used, corresponding to the design meridional streamlines. Back pressure was applied by closing the annular throttle built into the collector. Test points were taken at intervals of increasing back pressure until audible surging or a stall of such magnitude as to give excessive temperature fluctuations was reached. Complete operating curves were obtained for 50, 60, 70, 80, 90, and 100 percent of the design speed of 1400 feet per second.

RESULTS AND DISCUSSION

Over-all performance. - The standard compressor-performance map is shown in figure 9(a). The mass-weighted average total-pressure ratio P_5/P_1 is plotted against equivalent weight flow $W\sqrt{\theta}/\delta A_f$ for various percentages of design equivalent speed. At all speeds, peak weight flow coincides with peak pressure ratio, a characteristic obtained with similar compressor rotors. A range of operation is exhibited at all speeds, although pressure ratio drops off rapidly with decreasing weight flow at the higher speeds. The surge point shown by these curves was affected by system capacity and throttling characteristics. For instance, lower surge-free weight-flow points could be obtained with the throttle built into the collector than could be obtained with the butterfly valve located far downstream. When the collector throttle was used, a general unsteadiness was encountered, rather than a definite periodic surge. Because of a previous failure of the inlet guide vanes from fatigue, there was a reluctance to operate very long in this unsteady condition in order to find an audible surge point.

At design speed, the maximum weight flow was 24.84 pounds per second per square foot of frontal area at a pressure ratio of 4.7. Design weight-flow value was approximately 25.6 pounds per second. At higher speeds, there was very little increase in maximum weight flow since choking in the tail of the rotor limited the increase in weight flow with speed to that resulting from the increased relative total pressure.

In figure 9(b) the mass-weighted adiabatic efficiency of the rotor η_{ad} is presented as a function of equivalent weight flow for the various speeds. At tip speeds of 50, 60, and 70 percent of design, where the operation is basically subsonic, typical subsonic efficiency curves result and peak efficiencies are in the low 90's. At higher speeds, the open-throttle point is also the peak efficiency point, with a decrease occurring as back pressure is applied. At design speed, the peak efficiency of 0.85 is obtained for the pressure ratio of 4.7.

The mass-weighted average outlet flow angle β_5 is presented in figure 9(c). The range of outlet angle decreases with increasing tip speed.

In figure 9(d) the mass-weighted outlet Mach number is shown as a function of weight flow for the range of speed. As back pressure is applied, the axial velocity is reduced and thus the absolute velocity is also reduced. The absolute values of discharge Mach number are generally lower at a given pressure ratio than for the similar compressor of reference 4 because of the reduced wheel speed and greater deceleration in the blading. In general, however, the Mach number level increases as the

weight flow increases, and the change in Mach number with tip speed at a chosen weight flow is slight. From the standpoint of stator design, the large part of these curves which are at Mach numbers below 1.4 indicates that stator losses should be lower.

A summary of the over-all performance parameters given in figure 9 for the optimum operation at 90 percent of design speed reveals that at a weight flow of 23.6 pounds per square foot unit frontal area, the total-pressure ratio was 3.7, efficiency was 0.86, average outlet Mach number was 1.4, and average flow angle was 47°. This operating point has been chosen as design for subsequent stator investigations.

Inlet flow distribution. - The design angle distribution at the outlet of the guide vanes is shown by the dashed line in figure 10. The measured angle distribution for several weight flows is shown, and it can be seen that there is considerable overturning and that the distribution does not follow design very well. There was no evidence of choking in the guide vanes. In tests of a previous set of blades of identical specifications, the measured angle distribution agreed very well with design. It is quite possible that the measuring instrument was located in a wake or behind a poorly fabricated blade for these tests. Blade angle settings were checked at the conclusion of the test program and were found to be satisfactory.

The measured flow angles at station 3 immediately in front of the rotor are also given in figure 10. Again the angles are considerably higher than the design, particularly at the hub. At high back pressure, the angle of flow near the tip changes to indicate a large reduction of the axial velocity component. This type of profile is frequently indicative of tip stall or even of back flow in the rotor depending on the geometry involved. Unfortunately, attempts to run angle surveys at higher tip speeds were unsuccessful because the refrigerated air used froze the miniature claw. In addition, there were probably circumferential variations in the flow angle at both stations as a result of the guide-vane wakes. The overturning in the guide vanes is also a contributing factor to the high incidence angles at the rotor inlet, although the effect is slight.

Rotor-Outlet Surveys

All the results presented in this report were based on outlet surveys at station 5, 1 inch axially behind the compressor rotor. The radial distributions of pressure ratio, outlet Mach number, discharge angle, energy addition, axial Mach number, and the product of density and axial velocity ρV_{ax} are presented in figure 11 for a range of weight flow at 90 percent design speed. (Survey and blade-element data are presented at 90 percent design speed because this speed has been chosen as design for the subsequent stator investigation.)

Total-pressure ratio and absolute Mach number. - The total-pressure ratio is nearly uniform at wide-open throttle, although the isentropic design required higher values at the tip. Excessive losses at the tip are responsible for the fairly uniform pressure ratios shown. As back pressure is applied and weight flow decreases, the pressure ratio at the tip is relatively unchanged but drops off along the hub. This result accounts for the drop in mass-weighted total-pressure ratio with increasing back pressure. The same general trends are exhibited by the absolute Mach number, also shown in figure 11(a).

Axial Mach number. - The variation in absolute Mach number may be explained in terms of the axial component, shown in figure 11(c). As back pressure is applied, a shock on the axial component is forced forward in the rotor, with the axial Mach number decrease being greater along the hub than near the tip. Vector addition of this decreasing axial component to the relatively constant rotor speed, together with slight changes in direction of the relative flow, results in the absolute Mach numbers shown. By the nature of the velocity triangle, fairly large changes in the axial component have a smaller effect on the resultant velocity and angle.

Outlet flow angle. - The radial variation of flow discharge angle is given in figure 11(b). In general, the change in angle with increasing back pressure is small, and the same type of radial variation is maintained at all the weight flows. This radial variation in flow angle matches quite well with that of an untwisted radial-element stator blade.

ρV_{ax} Product. - The product of density and axial velocity is plotted against radius ratio in figure 11(b). This plot demonstrates the effect of the high axial velocity at the hub, which causes the ρV_{ax} product to be higher at the hub than at the tip. Inasmuch as the best blade-element efficiency is obtained along the hub, the mass-weighted average efficiency is improved by the greater flow in this region.

Comparative work input. - The comparative work input $C_p(T_5-T_0)/(RU_t)^2$ is plotted against radius ratio in figure 11(c). At the tip, there is very little change over the range of weight flow covered. At the hub, however, the work input decreases steadily as weight flow decreases. As will be shown later, this is caused, partly at least, by the underturning of the air (higher deviation angles) at the hub. In addition, there is a slight decrease in work input to be expected from the reduced prewhirl out of the guide vanes at lower weight flows, which should be applicable at all radii.

Static-pressure distribution over rotor. - In figure 12(a), the axial distribution of static-pressure ratio (observed pressure divided by inlet static pressure) along the flow path on the outer wall is presented for

open throttle at design speed (radial clearance of 0.028). Static pressure decreases between guide vanes and rotor and drops off sharply immediately in front of the rotor as a result of acceleration of the air caused by blade thickness and the upswept hub. The static pressure just inside the rotor rises very rapidly, then continues to rise at a decreasing rate to a peak value about 3/4 inch from the outlet. At this point, a slight increase in actual passage area (about 1 percent) occurs as a result of application of the boundary-layer allowance to the suction side only. A considerable expansion to a relatively low pressure is evident at this point, with supersonic relative Mach numbers resulting.

When back pressure is applied, the static-pressure ratio across the rotor is virtually unchanged except that the expansion in the tail of the rotor is eliminated. At this condition, the axial (relative) Mach number is subsonic.

The theoretical static-pressure distribution along the rotor-blade tip is shown by the dashed line in figure 12(a). A slight decrease in pressure occurs at the inlet as a result of the slight increase in Q specified. The prescribed static pressure then rises uniformly through most of the rotor although the rate of increase decreases near the rotor exit. This static-pressure distribution was for the original computed blade with boundary-layer allowance.

In figure 12(b) static-pressure profiles are presented for the maximum flow points at equivalent speeds of 50, 60, 70, 80, 90, and 100 percent of design. At the lower speeds, nearly all the pressure rise occurs in the front of the rotor; whereas, at higher speeds, the initial rate of pressure rise remains the same but persists over a greater axial length. At all speeds there is some expansion in the tail of the rotor at wide-open throttle. By careful throttle control, the expansion could be eliminated as back pressure increased without affecting the pressure over the front of the rotor.

Blade-Element Performance at 90 Percent Design Speed

Efficiency. - In figure 13(a) a comparison of adiabatic and momentum efficiency is shown as computed along the original meridional streamlines for the test points obtained at 90 percent design speed. Adiabatic efficiency is, of course, based on observed pressure ratio and temperature rise. On the other hand, no outlet-temperature measurements are required for momentum efficiency, as shown by its definition:

$$\eta_m = \frac{2a_{0,1}^2 \left[\left(\frac{P_5}{P_3} \right)^{\frac{\gamma-1}{\gamma}} - 1 \right]}{(\gamma - 1)U_t \left(R_5 V_{tan,5} + R_3 V_{tan,3} \right)}$$

[redacted]

(or, the ratio of ideal work to achieve the pressure ratio P_5/P_3 to the actual work as determined by change in moment of momentum of the fluid). For this reason, a comparison of momentum efficiency and adiabatic efficiency shows the quality of the temperature-rise measurements and also indicates the accuracy of angle determination. ($V_{tan,5}$ is the tangential component of the observed outlet velocity.) As shown by figure 13(a), the shape and trend of the curves are in good agreement, although the absolute values may vary by 3 or 4 percent. In general, momentum efficiency is higher than adiabatic except at the hub where adiabatic efficiency at times exceeds 100 percent, probably as a result of deviation of the true streamlines from the assumed meridional streamlines. It can be seen that the efficiency along the hub is very high and that there is no evidence of separation from the hub at the open-throttle points. At high back pressures, efficiency is not affected much at the tip but is reduced considerably at the hub.

Relative Mach number. - The inlet and outlet relative Mach numbers at 90 percent design speed, as computed for the seven meridional streamlines, are given in figure 13(b). As expected from the small change in weight flow, the inlet relative Mach number, which was computed from rotor speed and inlet absolute velocity, does not change much with weight flow but does increase uniformly with radius ratio. The maximum value of 1.39 at the blade tip at 90 percent design speed is lower than that of the supersonic compressors of references 2 to 4. The outlet relative Mach number is almost identical to the axial component of Mach number shown in figure 11(c) because the blading turns essentially to the axial direction. For the open-throttle points, the outlet relative Mach number is barely supersonic and increases uniformly from tip to hub. As back pressure is applied, both inlet and outlet relative Mach numbers are decreased as weight flow changes. The radial test points nearest the wall were 0.13 inch from the outer wall and 0.17 inch from the inner wall. Both points appear to be outside the wall boundary layers, and it is indicated that there is little, if any, separation on the high-curvature portion of the hub. Comparison of the inlet and outlet relative Mach numbers shows large decelerations along the tip at all flows with slight deceleration at the hub except at the higher weight flows.

Incidence angle and deviation angle. - The incidence angle presented in figure 13(c) is the difference between the measured mean-line blade angle and the flow angle computed at station 3 immediately in front of the rotor (angle measurements are with respect to axial direction). Positive incidence angles signify flow angles larger than the blade angle. Through an error in fabrication, the actual blade angles are lower than design by about 5° at the tip and less at the hub. As a result, at design weight flow the angle of incidence would be excessive, and the wedge angle of the pressure surface is greater than that which would sustain an attached oblique shock wave. Consequently, a detached wave system could be expected, with a strong shock standing at the channel entrance. The

losses through this shock system and the loss in effective area due to separation may be great enough to affect the area variation laid out for isentropic flow, even with the boundary-layer allowance. In a channel skewed at an angle to the axis of rotation, a normal shock may occur without an apparent discontinuity in static pressure because of the averaging action of the static-pressure taps.

As shown in figure 13(c), high-incidence angles prevailed at all weight flows and, as expected, increased with decreasing weight flow.

Deviation angle is defined as the difference between the outlet relative flow direction and the blade mean-line angle. Because of the application of the boundary-layer allowance, the actual blade angle at discharge was 2° beyond axial. According to convention, positive deviation angle signifies flow angles lower than the blade angle, or under-turning.

At the tip, the flow turns slightly past the blade (negative deviation angle) and is relatively unaffected by changes in back pressure. The roll-up of casing boundary layer caused by the scraping action of the tip could displace the main flow direction toward the suction surface and result in this slight overturning. At the mean radius, the flow is always underturned a few degrees. At the hub, the trend is toward higher turning, but in this region the greatest effects of back pressure are evident. At open throttle, a negative deviation of about 1° occurs, while at higher back pressures a positive deviation of as much as 7° is apparent.

Recovery factor. - The ideal relative total-pressure ratio, the observed relative total-pressure ratio, and the ratio of the latter to the former, called "recovery factor", are presented for the seven meridional streamlines in figure 13(d). The ideal relative total-pressure ratio is a function of the change in radius and the speed only, as shown in the definitive equation

$$\left(\frac{P_5'}{P_3'}\right)_{id} = \left\{1 + \frac{\gamma - 1}{2}\left(\frac{U_t R_5}{a_0'}\right)^2\left[1 - \left(\frac{R_3}{R_5}\right)^2\right]\right\}^{\frac{\gamma}{\gamma-1}}$$

For this particular rotor, the value of ideal relative total-pressure ratio at the hub is quite large because of the large change in radius.

The actual relative total-pressure ratio may be computed from known parameters as follows:

$$\frac{P_5'}{P_3'} = \frac{P_5}{P_3} \times \frac{P_3}{P_3'} \times \frac{P_3}{p_3} \times \frac{p_5}{P_5} \times \frac{P_5'}{p_5}$$

where the ratio p/P may be found from tables or from the relation

$$\frac{p}{P} = \left(1 + \frac{\gamma - 1}{2} M^2\right)^{-\frac{\gamma}{\gamma-1}}$$

at the particular Mach number being considered. A plot of relative total-pressure ratio based on measurements at station 5 is also given in this figure for comparison with the ideal. At the tip a considerable loss exists, as shown by the difference between ideal and actual relative total-pressure ratio, and there is little change with weight flow. At the hub, however, the actual ratio approaches the ideal at low back pressures but falls off as back pressure is increased.

The recovery factor, which is directly analogous to the recovery factor of stationary cascades and supersonic inlets, shows the same trends exhibited by adiabatic efficiency. However, the absolute values of recovery factor are lower as a result of the large amount of energy being added while the pressure losses are occurring. Again, recovery factor is much higher at the hub than at the tip and is decreased as back pressure is increased at the hub.

Blade-Element Performance at Open Throttle

Efficiency. - In figure 14(a) the adiabatic and momentum efficiency are plotted against radius for open throttle over the entire range of speed covered. At low speeds, 50, 60, and 70 percent, the efficiency is very high over all the passage except near the tip, where tip effects are predominant. As tip speed is increased (hence inlet relative Mach number and blade loading), efficiency falls off uniformly from hub to tip and the absolute value of efficiency drops.

Relative Mach number. - In figure 14(b) the inlet and outlet relative Mach numbers are presented. Inlet relative Mach number increases uniformly with speed and radius ratio. At speeds below 90 percent, the outlet relative Mach number averages approximately 1.0, demonstrating that choking is occurring either in the tail of the rotor or at the measuring station. At speeds above 90 percent, a Mach number above 1.0 can be sustained in the short straight annulus. At these speeds, Mach number is considerably higher at the hub than at the tip. Comparison of the inlet and outlet relative Mach number shows that at the lowest speed there is some acceleration at both hub and tip. At higher tip speeds, there is always deceleration along the tip, increasing in amount as speed increases. At the hub the air accelerates through the rotor; this fact probably accounts for the improved blade-element efficiency in this region.

Incidence angle and deviation angle. - As mentioned previously, incidence angle (fig. 14(c)) is based on the mean line of the existing blade. At low speeds, incidence angle is relatively low but increases toward the blade tip because of the incorrect blade angle at the tip. At higher speeds, increases in weight flow with speed are slight, resulting in small change in incidence angle. Also, the variation from hub to tip is less than for lower speeds.

The deviation angles, also presented in figure 14(c), are undoubtedly affected by the expansion in the tail of the rotor but do exhibit trends that may possibly be interpreted in the light of visual studies of secondary flows. At speeds up to 80 percent, the flow is underturned at the tip, possibly as a result of leakage through the clearance space which forces the main stream toward the pressure surface. At the higher speeds a scraping action may occur, as discussed in reference 10. The roll-up of low-energy air by this scraping, possibly in the form of a vortex on the pressure surface of the blade, would force the main stream toward the suction surface, resulting in negative deviation angles. At the hub, there is normally an accumulation of low-energy air in the corner formed by the suction surface and hub. However, at open throttle, there is no evidence of separation on the hub and the deviation angles are negative.

Recovery factor. - In figure 14(d) the ideal relative total-pressure ratio, the observed relative total-pressure ratio (based on outlet surveys), and the ratio of observed to ideal total-pressure ratio, or recovery factor, are presented for the open-throttle points. From the curves of ideal relative total-pressure ratio, it is apparent that the contribution of the increase in radius along the lower streamlines is much greater at higher tip speeds. In general, the observed relative pressure ratio follows the trend of the ideal except at the tip at 50 percent speed where tip-clearance losses probably prevail. At each higher tip speed, the difference between ideal and observed pressure ratio is increased. This loss shows up in the recovery factor, which is much lower at high speeds and near the tip. At the low speeds the optimum recovery factor is attained about 1/3 span from the outer shroud.

SUMMARY OF RESULTS

As a result of an investigation in air of the over-all performance of an impulse-type supersonic-compressor rotor, without stators, with a hub-tip ratio of 0.6 and turning to the axial direction, the following facts may be stated:

1. At the design speed of 1400 feet per second, maximum weight flow, adiabatic efficiency, and pressure ratio occurred at a single operating point having values of 24.84 pounds per second per square foot of frontal area, 0.85, and 4.7, respectively.

2. Consideration of the rotor-outlet Mach numbers showed that the optimum match point for stator design was at speeds lower than design rotor speed. For instance, at 1260 feet per second (90 percent), the stator-inlet Mach number would be 1.4 at an average angle of 47°. At this point, the rotor efficiency was 0.86 and the pressure ratio was 3.7.

3. The radial distributions of total-pressure ratio, absolute Mach number, and flow angles at 90 percent speed were reasonably uniform and were therefore considered suitable for stator work.

4. The rotor operated at excessive incidence angles at the higher tip speeds; and as a result, an external shock configuration, accompanied by a strong shock, appeared at the rotor entrance. Therefore, the recovery factor at the tip was quite poor at the inlet Mach numbers involved.

Lewis Flight Propulsion Laboratory
National Advisory Committee for Aeronautics
Cleveland, Ohio, March 2, 1954

[redacted]

APPENDIX - SYMBOLS

The following symbols are used in this report:

A_f	frontal area, sq ft
a	sonic velocity, ft/sec
C_p	specific heat of air, Btu/(lb)($^\circ$F)
M	Mach number
n	number of blades
p	static pressure, in. Hg abs
P	total pressure, in. Hg abs
Q	velocity/$a_{0,1}$
R	radius/radius at tip
r_t	tip radius, in.
T	temperature, $^\circ$F abs
t	blade thickness perpendicular to axis, in.
U_t	tip speed, ft/sec
V	velocity, ft/sec
W	weight flow, lb/sec
β	flow angle, deg
γ	ratio of specific heats
δ	ratio of inlet total pressure to NACA standard sea-level pressure (29.92 in. Hg)
η_{ad}	adiabatic efficiency
η_m	momentum efficiency
θ	ratio of inlet total temperature to NACA standard sea-level temperature (518.4° R)
ρ	weight density, lb/cu ft

[redacted]

Subscripts:

0	stagnation value
1	in inlet tank
2	behind guide vanes
3	in front of rotor
5	behind rotor
ax	axial component
e	entrance
id	ideal
tan	tangential component

Superscript:

'	relative

REFERENCES

1. Wright, Linwood C., and Klapproth, John F.: Performance of Supersonic Axial-Flow Compressors Based on One-Dimensional Analysis. NACA RM E8L10, 1949.

2. Ullman, Guy N., Hartmann, Melvin J., and Tysl, Edward R.: Experimental Investigation of a 16-Inch Impulse-Type Supersonic-Compressor Rotor. NACA RM E51G19, 1951.

3. Jacklitch, John J., Jr., and Hartmann, Melvin J.: Investigation of 16-Inch Impulse-Type Supersonic Compressor Rotor with Turning Past Axial Direction. NACA RM E53D13, 1953.

4. Tysl, Edward R., Klapproth, John F., and Hartmann, Melvin J.: Investigation of a Supersonic-Compressor Rotor with Turning to Axial Direction. I - Rotor Design and Performance. NACA RM E53F23, 1953.

5. Hartmann, Melvin J., and Tysl, Edward R.: Investigation of a Supersonic-Compressor Rotor with Turning to Axial Direction. II - Rotor Component Off-Design and Stage Performance. NACA RM E53L24, 1954.

6. Stewart, Warner L., Schum, Harold J., and Whitney, Warren J.: Investigation of Turbines for Driving Supersonic Compressors. I - Design and Performance of First Configuration. NACA RM E52C25, 1952.

7. Lieblein, Seymour, Schwenk, Francis C., and Broderick, Robert L.: Diffusion Factor for Estimating Losses and Limiting Blade Loadings in Axial-Flow-Compressor Blade Elements. NACA RM E53D01, 1953.

8. Lieblein, Seymour: Turning-Angle Design Rules for Constant-Thickness Circular-Arc Inlet Guide Vanes in Axial Annular Flow. NACA TN 2179, 1950.

9. Lieblein, Seymour, and Ackley, Richard H.: Secondary Flows in Annular Cascades and Effects on Flow in Inlet Guide Vanes. NACA RM E51G27, 1951.

10. Hansen, Arthur G., Herzig, Howard Z., and Costello, George R.: A Visualization Study of Secondary Flows in Cascades. NACA TN 2947, 1953.

[redacted]

TABLE I. - COORDINATES OF SUPERSONIC-COMPRESSOR ROTOR BLADE

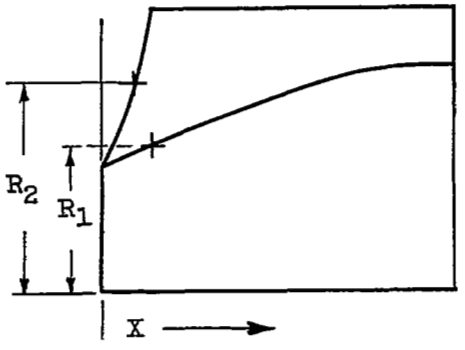

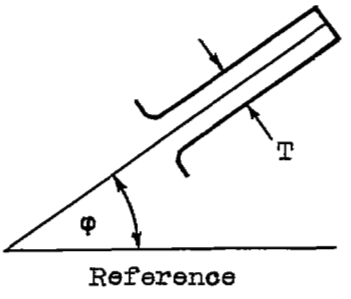

Blade coordinates			Hub contour coordinates		Leading-edge coordinates	
X	φ	T	X	R_1	X	R_2
0	0° 0' 0"	0.148	0	4.639	0.005	4.643
.20	3° 56' 37"	.142	.2	4.736	.05	4.730
.40	7° 34' 58"	.130	.4	4.836	.10	4.832
.60	10° 49' 09"	.112	.6	4.936	.15	4.944
.80	13° 35' 56"	.158	.8	5.035	.20	5.068
1.00	15° 59' 21"	.228	1.0	5.136	.25	5.195
1.20	18° 05' 02"	.296	1.2	5.235	.30	5.338
1.40	19° 54' 53"	.348	1.4	5.335	.35	5.496
1.60	21° 28' 05"	.388	1.6	5.434	.40	5.668
1.80	22° 48' 07"	.416	1.8	5.534	.45	5.860
2.00	23° 57' 08"	.432	2.0	5.634	.50	6.067
2.20	24° 56' 46"	.438	2.2	5.734	.55	6.298
2.40	25° 46' 11"	.434	2.4	5.833	.60	6.509
2.60	26° 25' 40"	.426	2.6	5.932	.65	6.931
2.80	26° 57' 53"	.410	2.8	6.033	.70	7.376
3.00	27° 23' 24"	.392	3.0	6.132	.75	7.975
3.20	27° 43' 49"	.364	3.2	6.232		
3.40	27° 58' 51"	.326	3.4	6.327		
3.60	28° 10' 24"	.286	3.6	6.423		
3.80	28° 19' 0"	.240	3.8	6.517		
4.00	28° 25' 27"	.198	4.0	6.606		
4.20	28° 30' 01"	.154	4.2	6.681		
4.40	28° 32' 42"	.116	4.4	6.738		
4.60	28° 33' 14"	.082	4.6	6.781		
4.80	28° 32' 10"	.054	4.8	6.811		
5.00	28° 29' 28"	.032	5.0	6.831		
5.127	28° 27' 03"	.020	5.127	6.840		

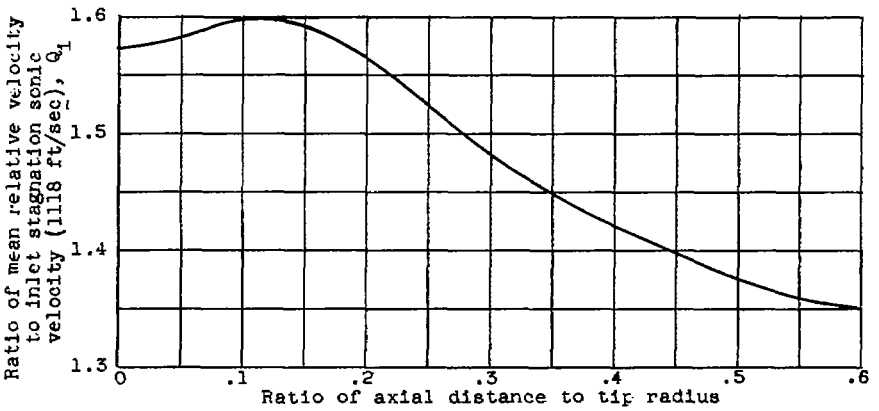

Figure 1. - Prescribed variation of mean velocity ratio with axial distance.

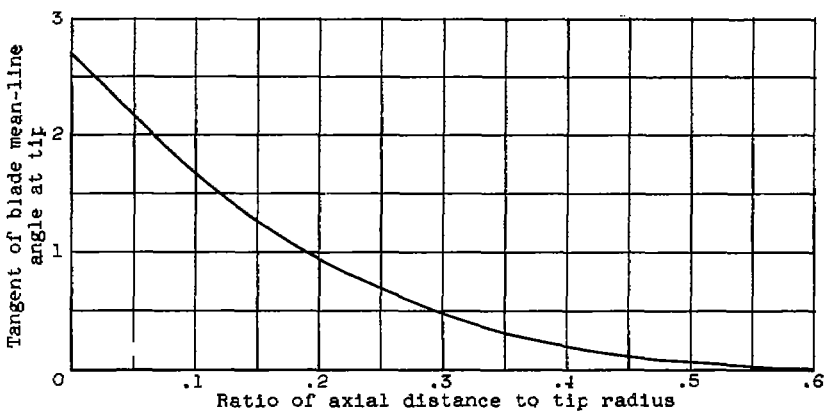

Figure 2. - Prescribed mean flow direction at tip.

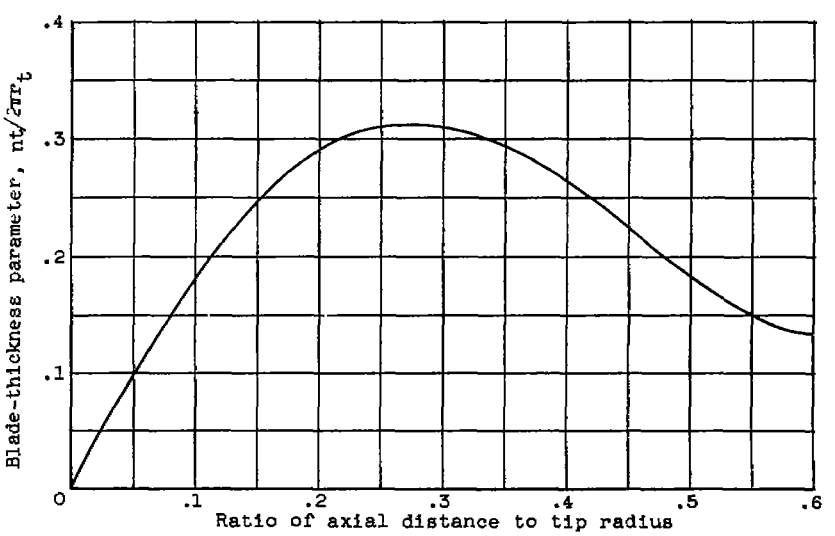

Figure 3. - Prescribed variation of blade thickness with axial distance.

[redacted]

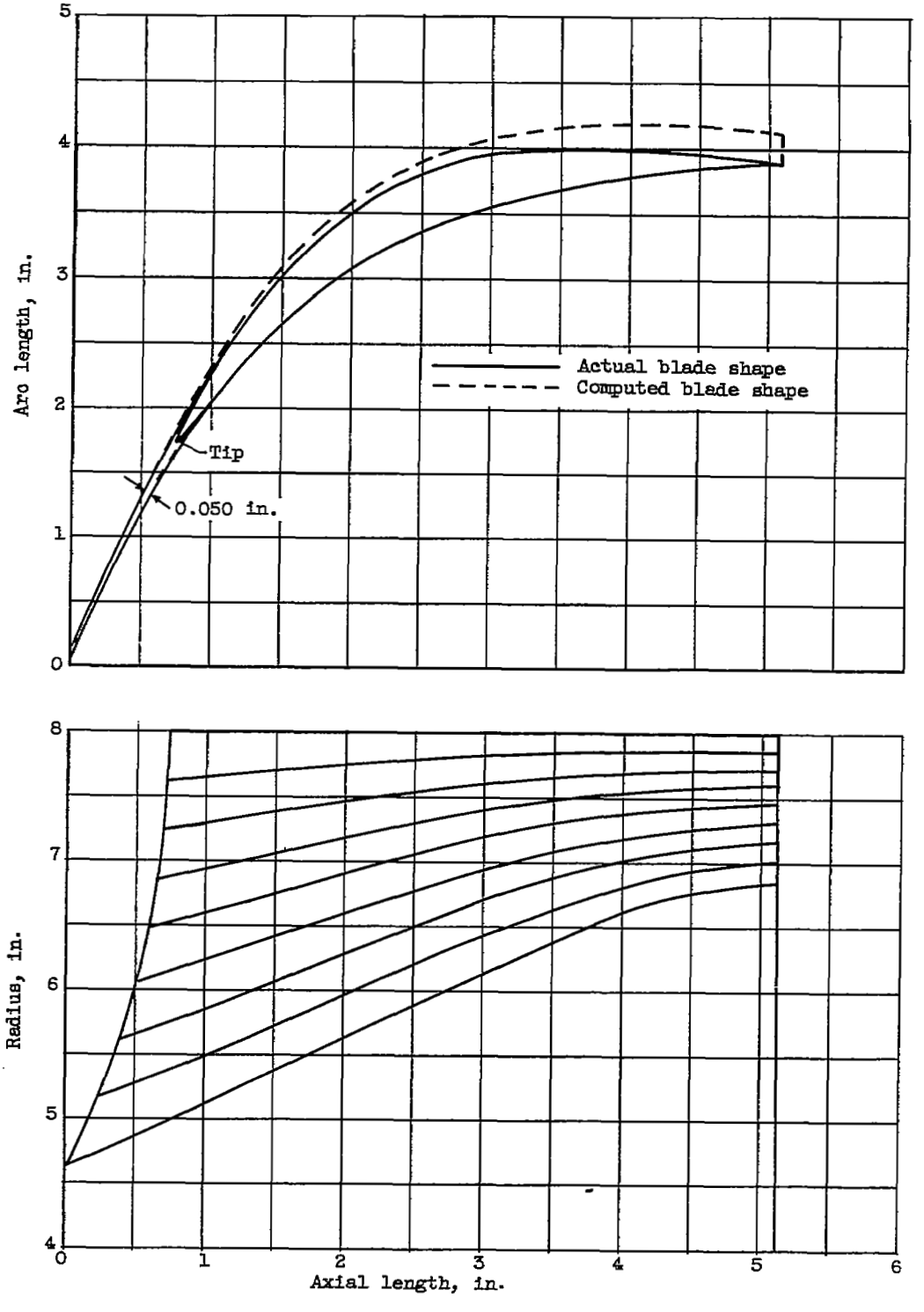

Figure 4. - Meridional section and blade layout of rotor.

[redacted]

Figure 5. - Supersonic-compressor rotor.

[redacted]

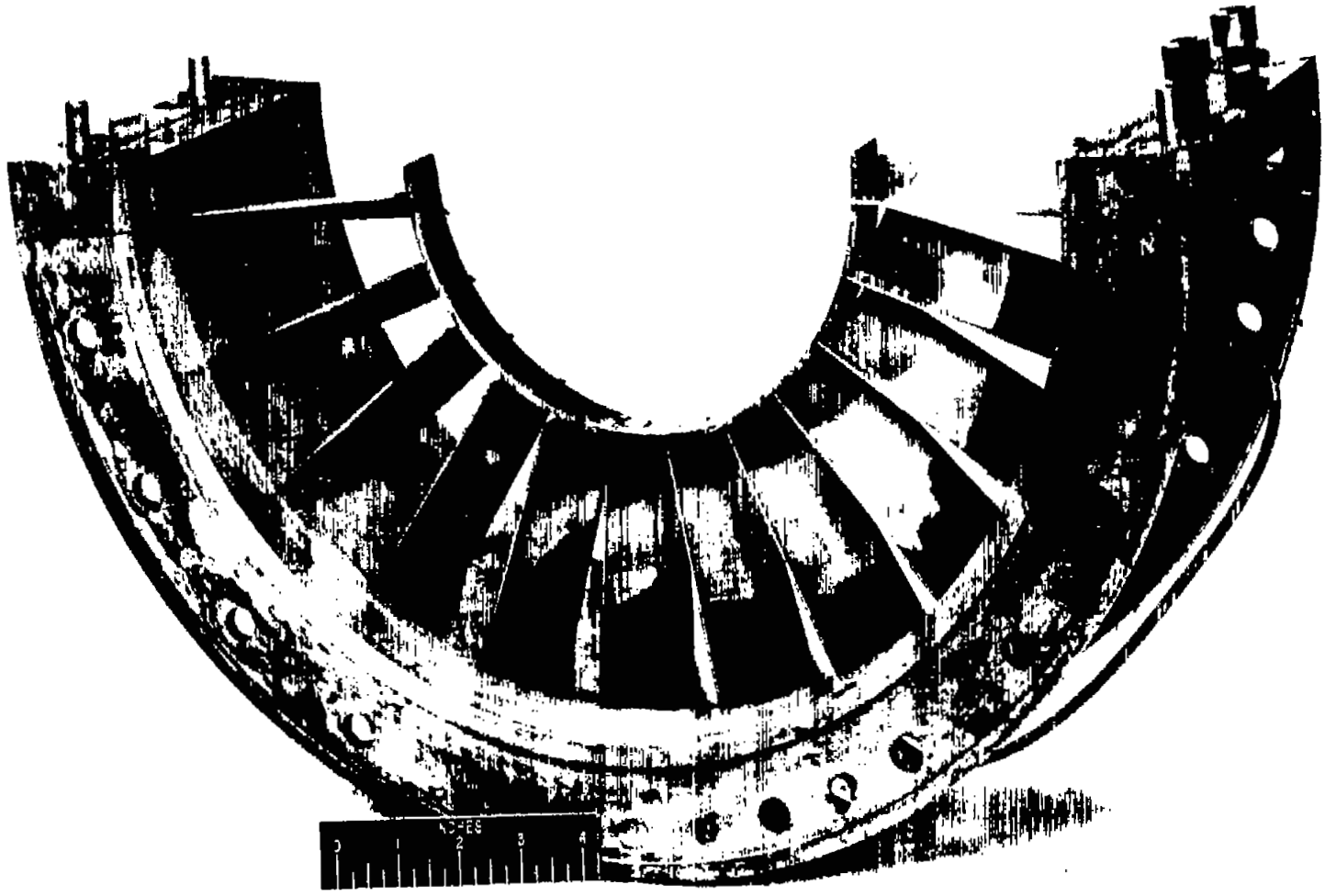

C-34129

Figure 6. - Guide-vane installation.

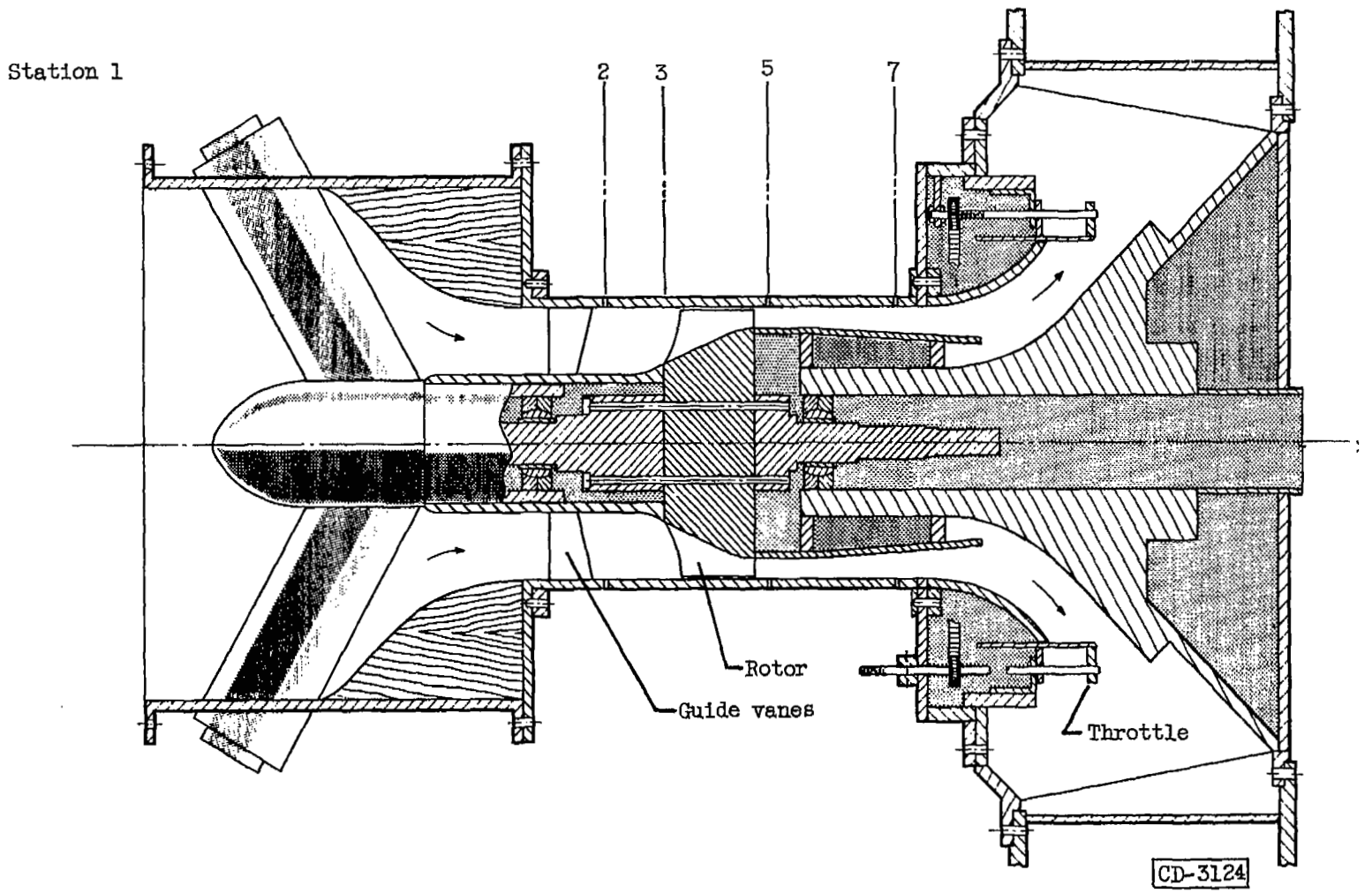

Figure 7. - Schematic sketch of rotor installed in variable-component test rig.

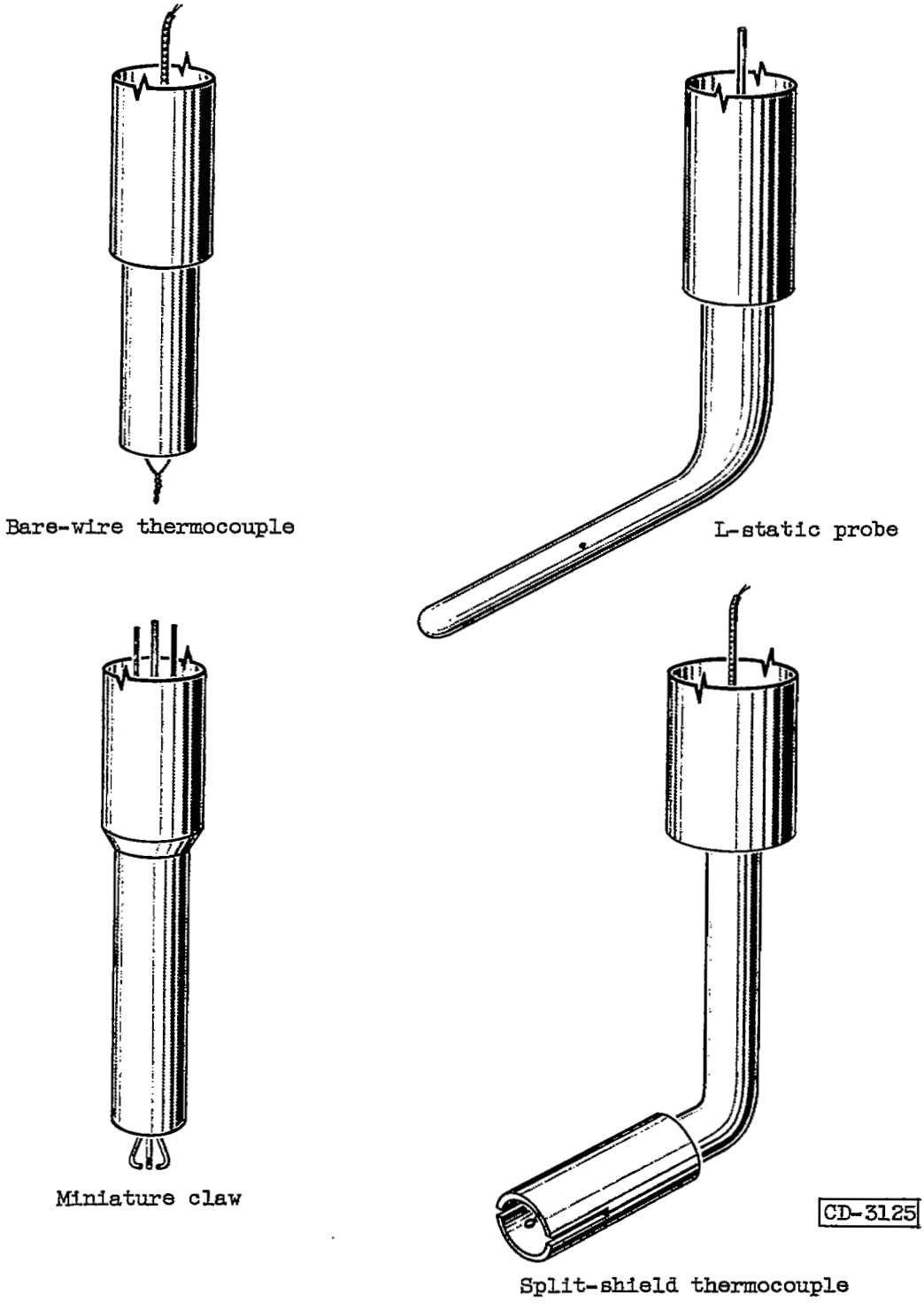

Figure 8. - Schematic sketches of instruments used in tests of rotor.

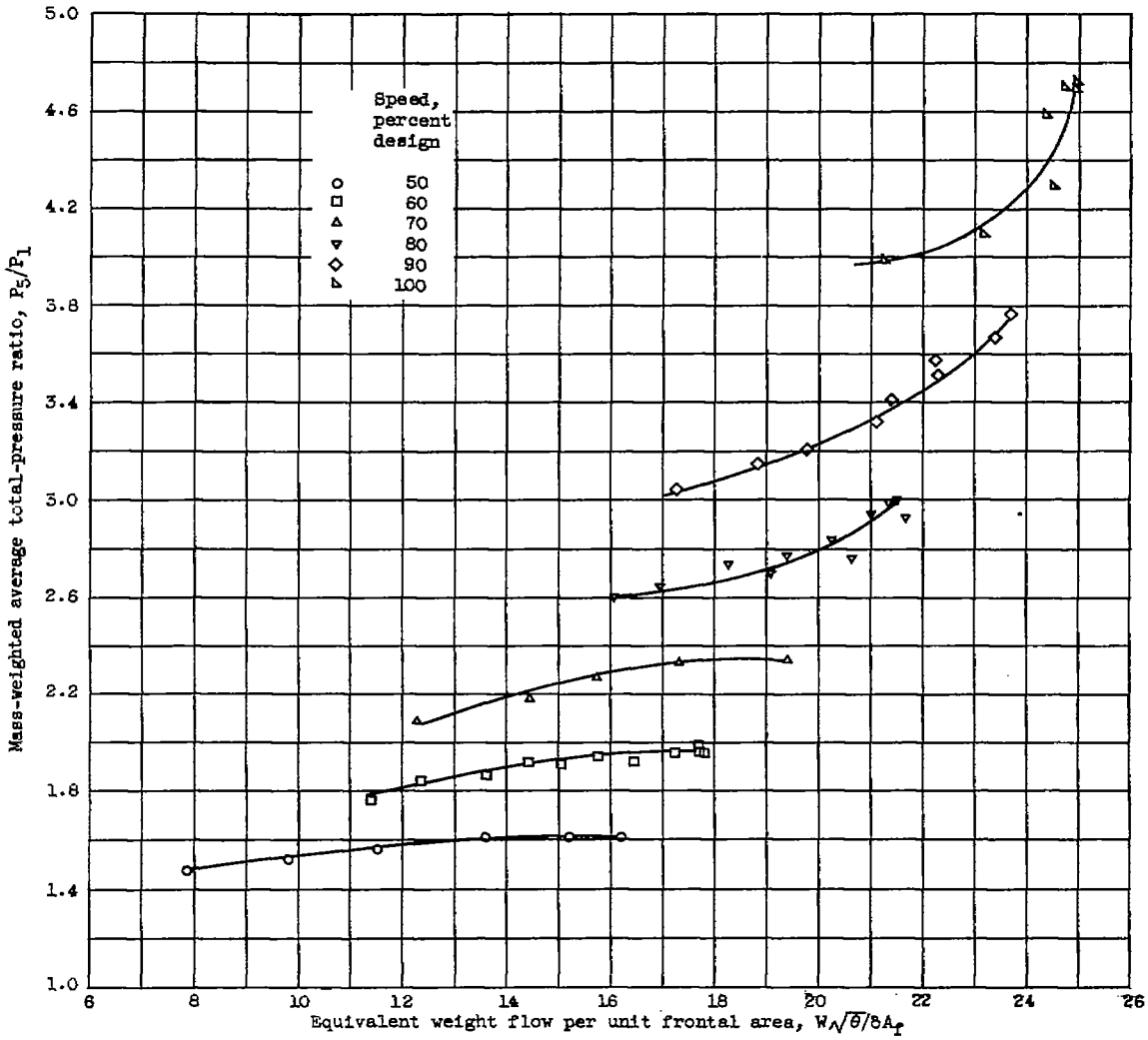

(a) Mass-weighted average total-pressure ratio.

Figure 9. - Over-all performance of supersonic-compressor rotor.

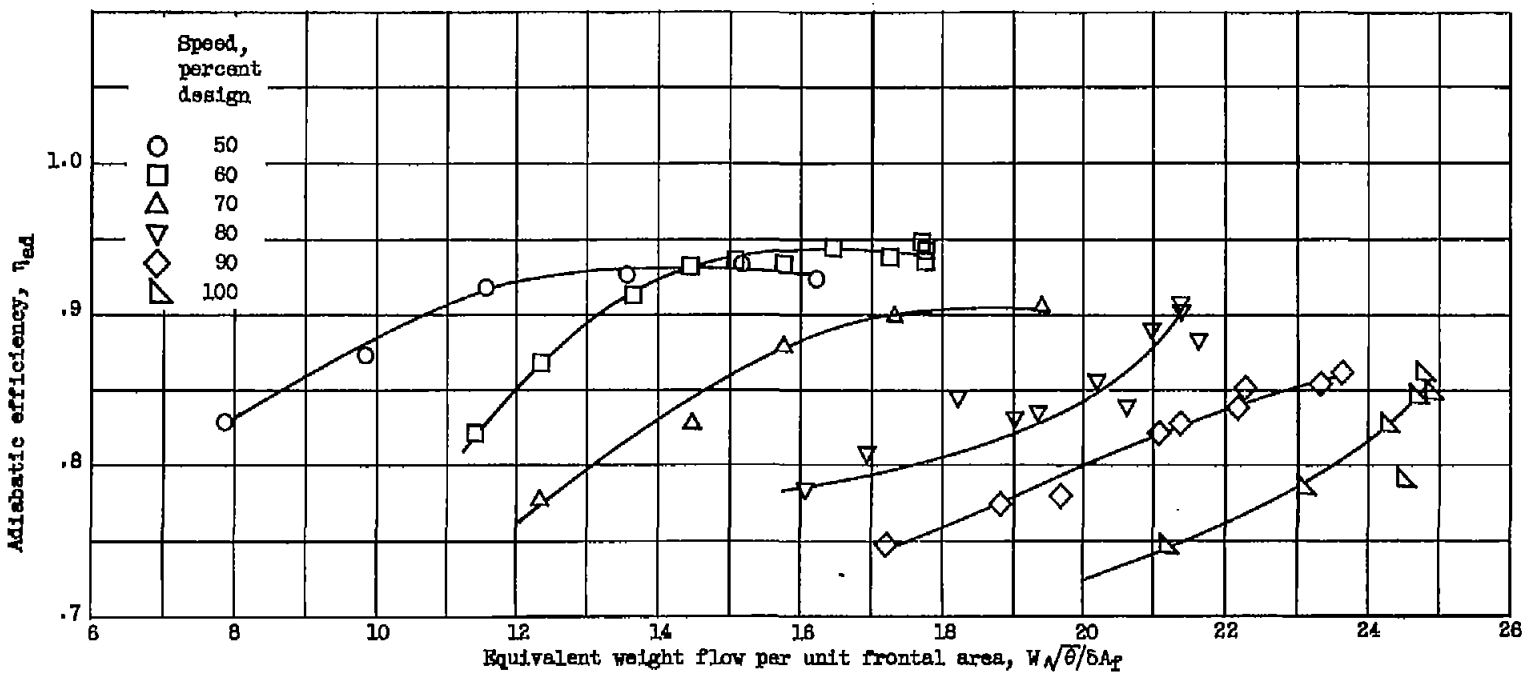

(b) Adiabatic efficiency.

Figure 9. - Continued. Over-all performance of supersonic-compressor rotor.

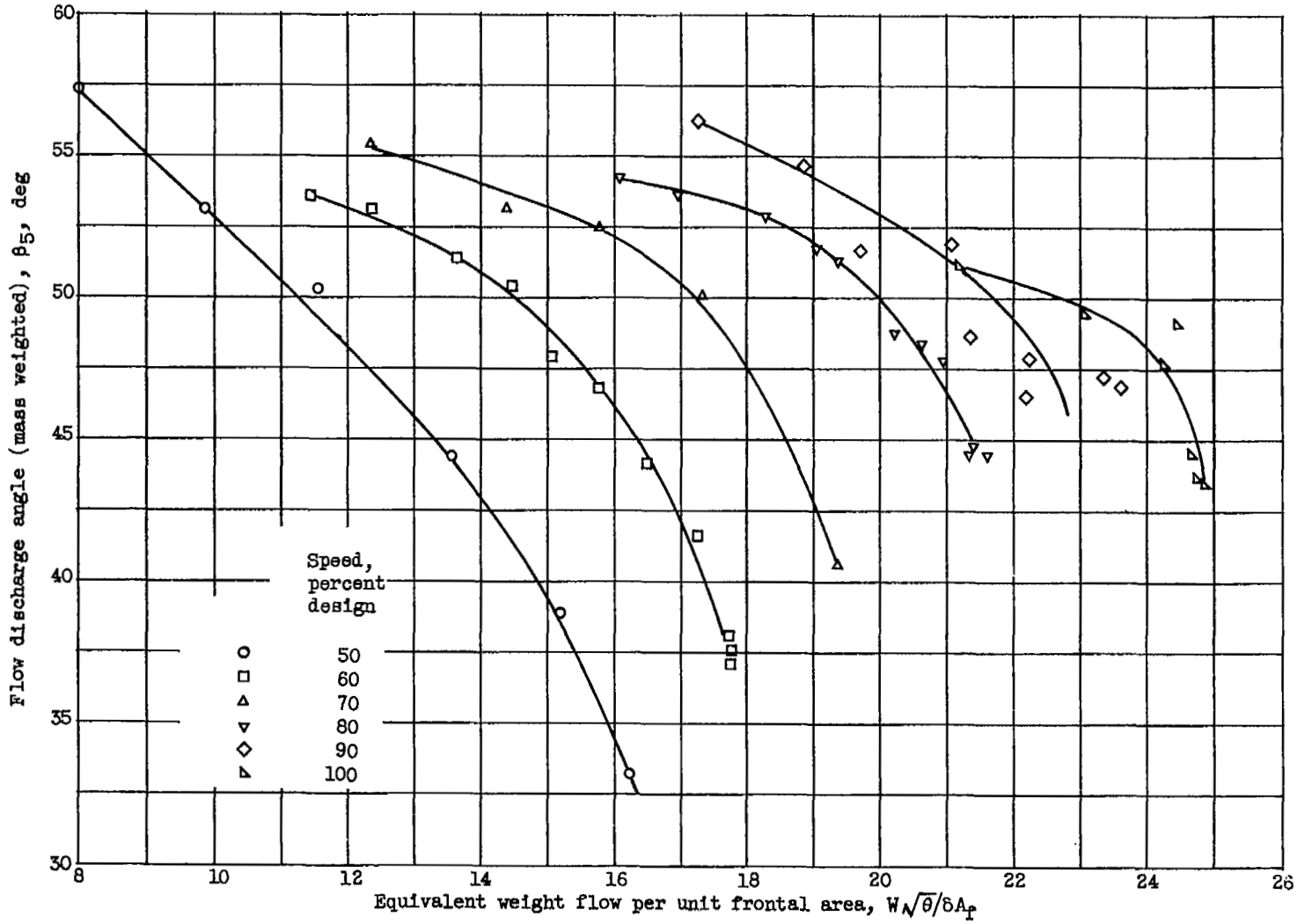

(c) Discharge flow angle.

Figure 9. - Continued. Over-all performance of supersonic-compressor rotor.

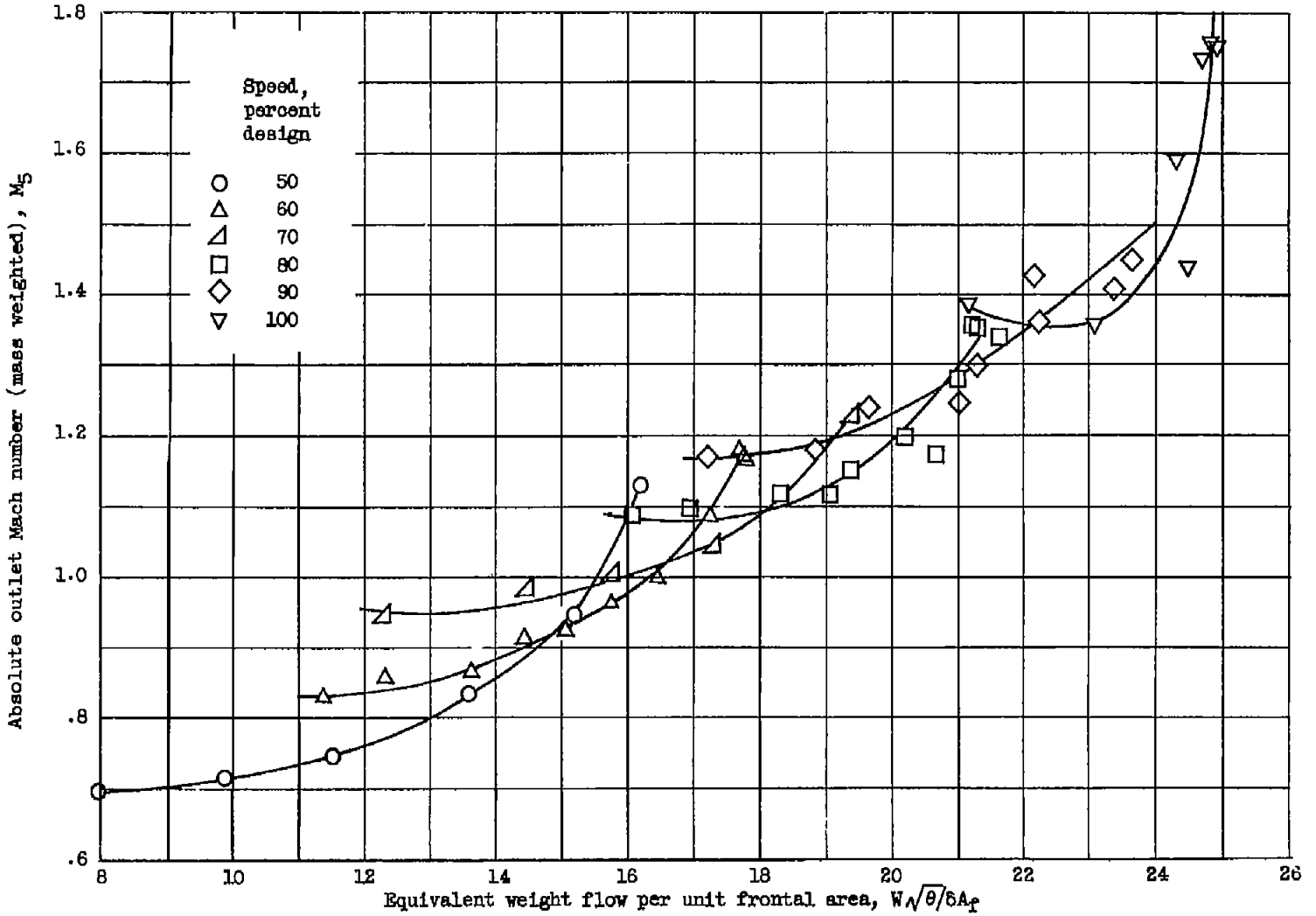

(d) Average discharge Mach number.

Figure 9. - Concluded. Over-all performance of supersonic-compressor rotor.

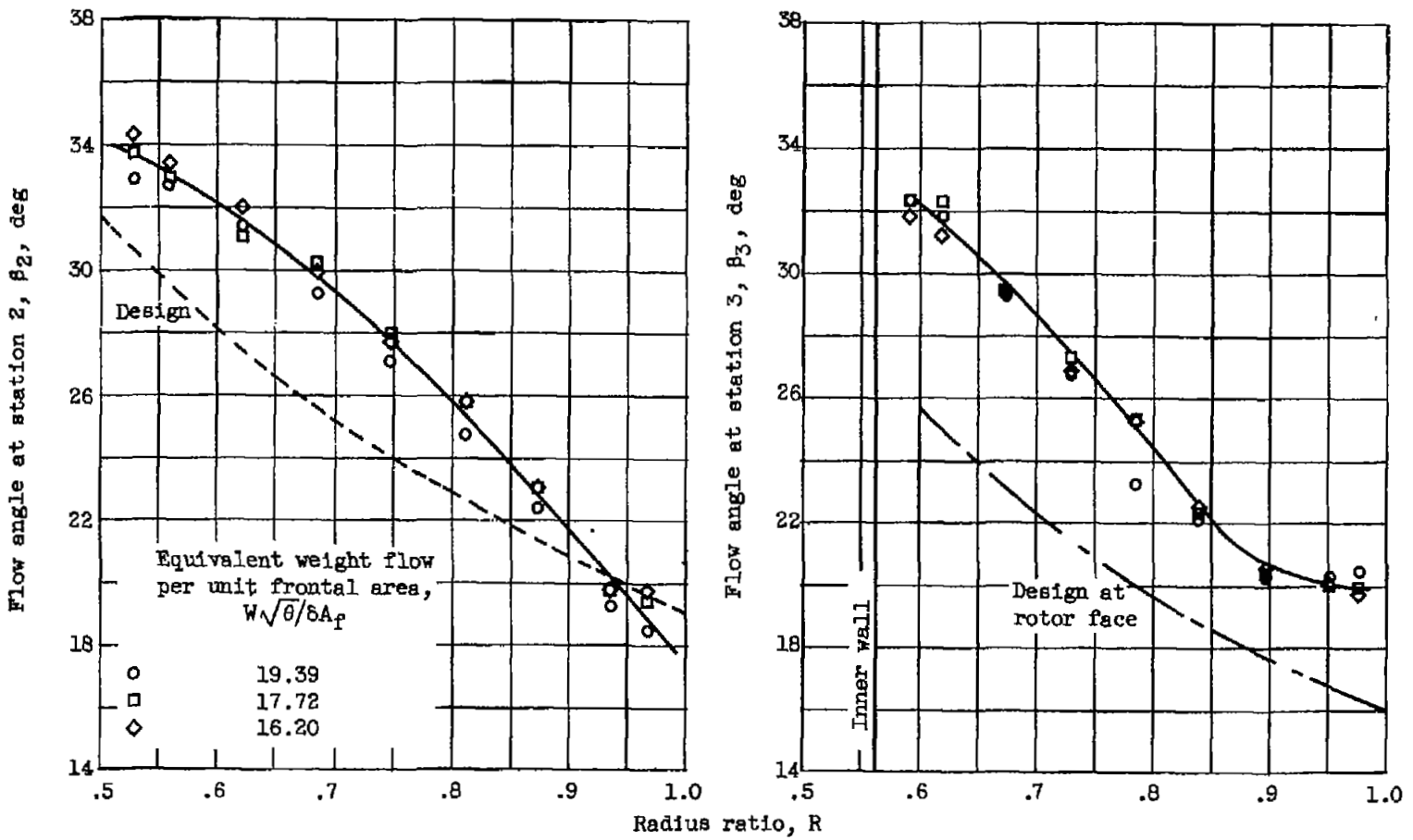

Figure 10. - Angle distribution behind guide vanes and in front of rotor.

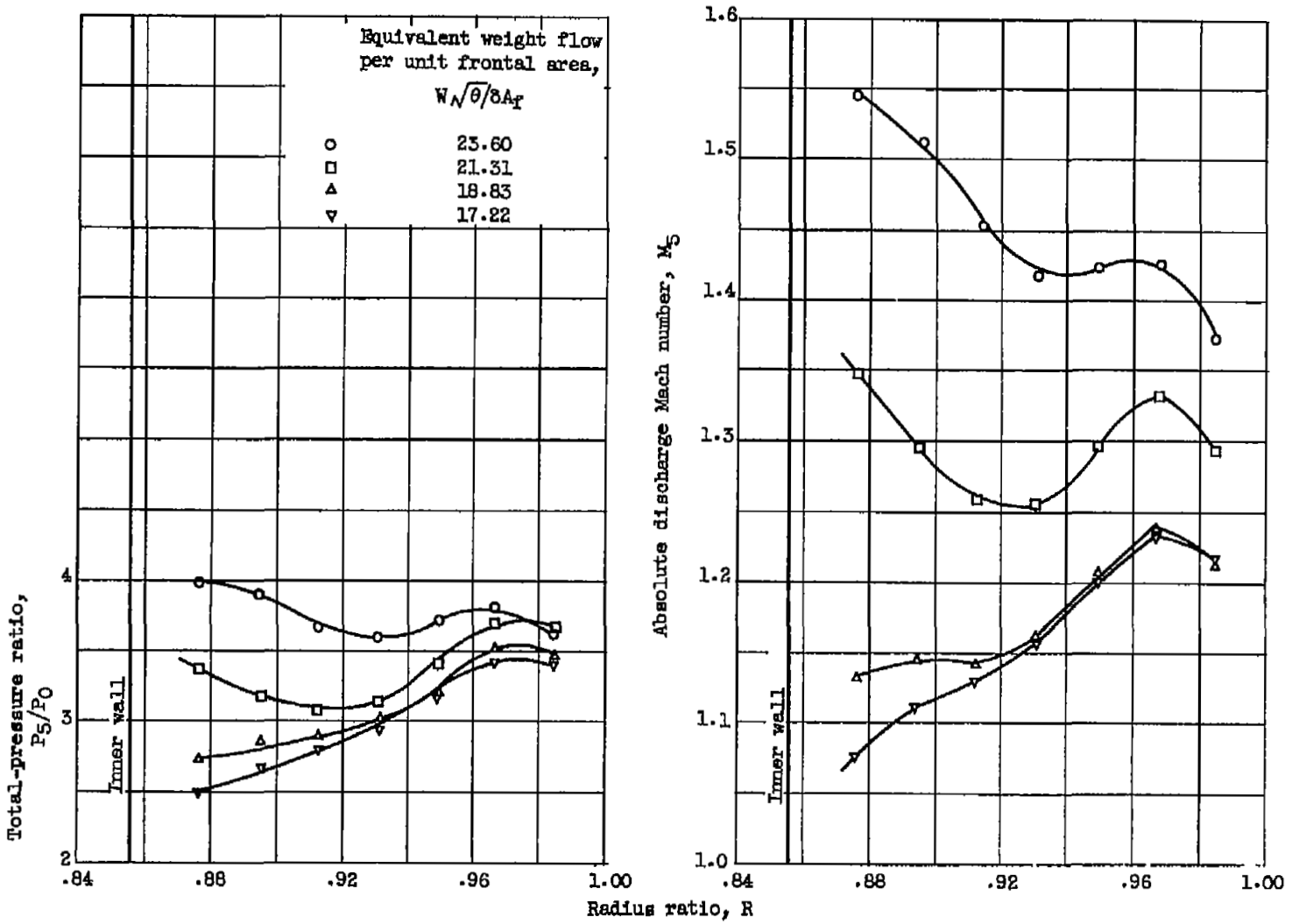

(a) Pressure ratio and Mach number.

Figure 11. - Outlet surveys at 90 percent design speed.

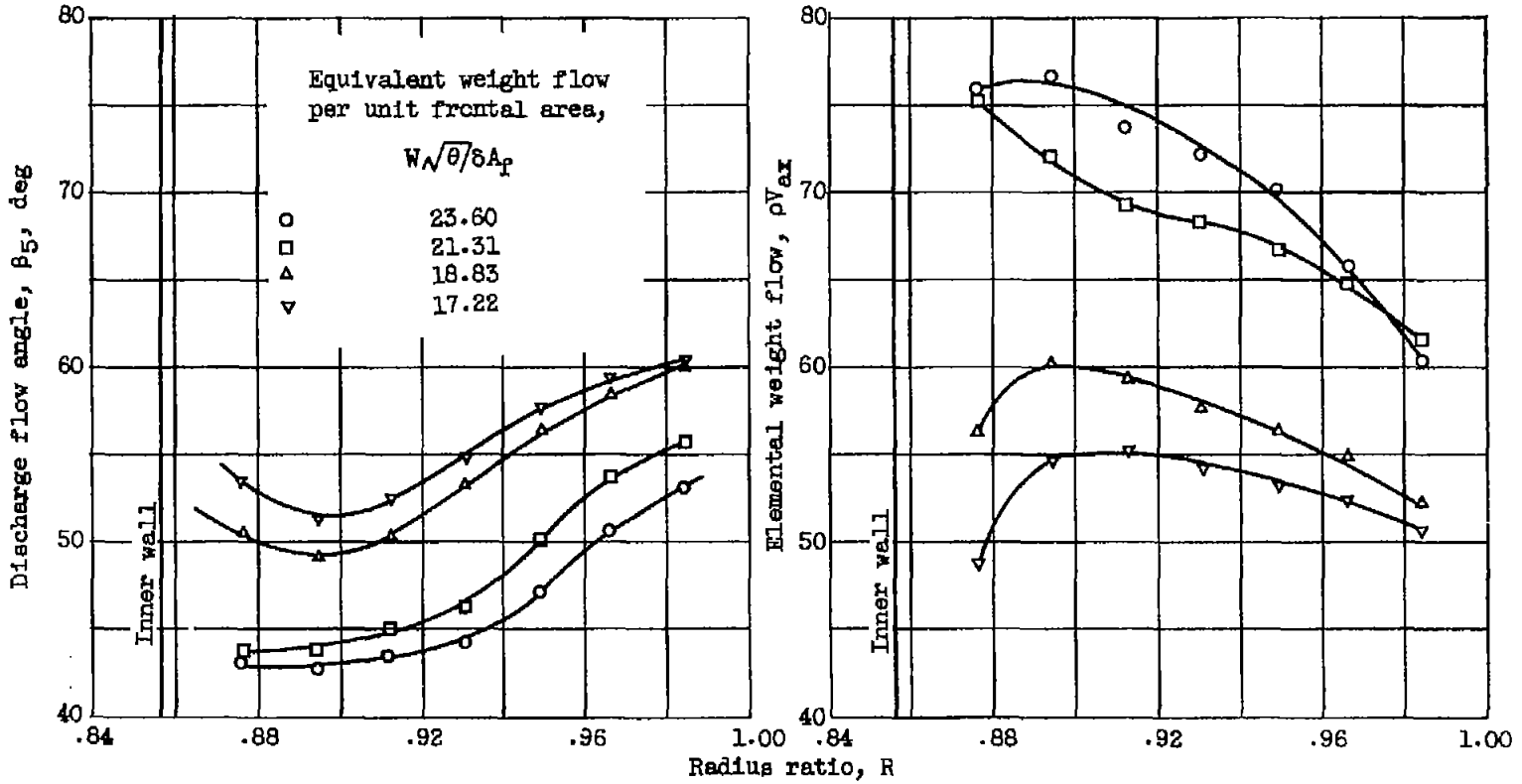

(b) Flow angle and elemental weight flow.

Figure 11. - Continued. Outlet surveys at 90 percent design speed.

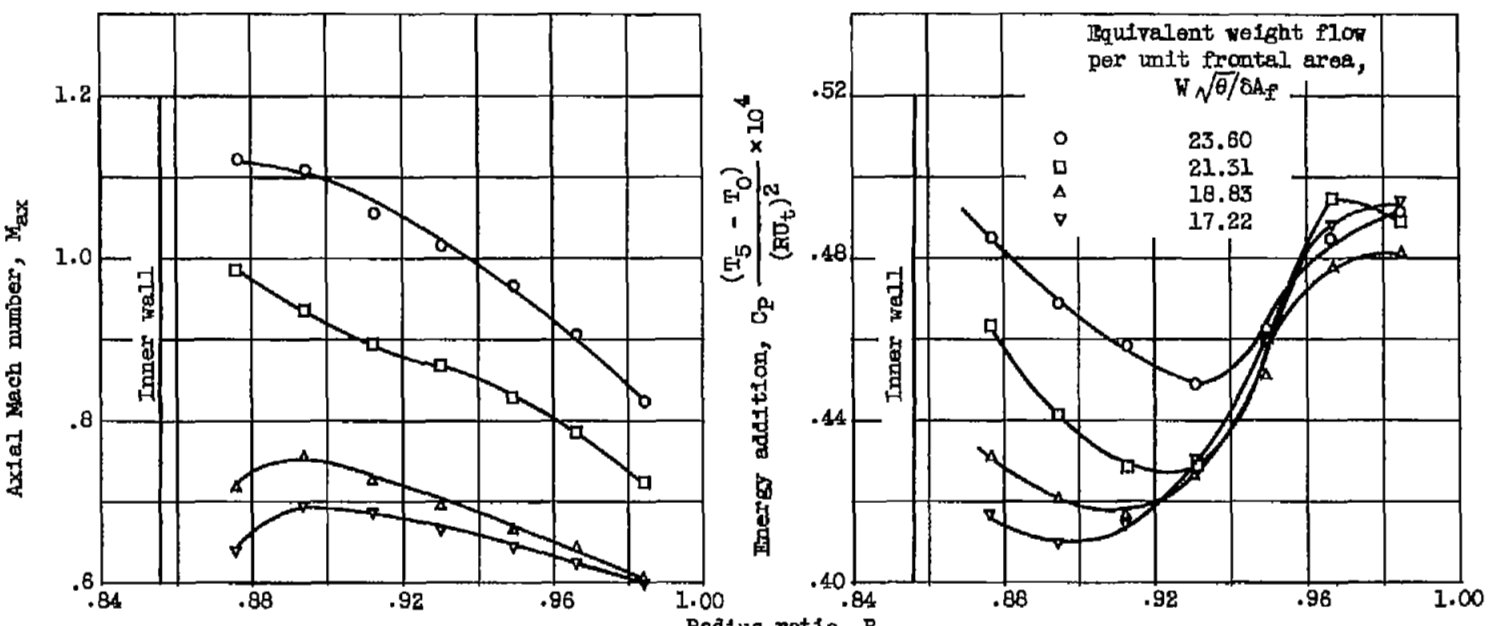

(c) Axial component of Mach number and energy addition.

Figure 11. - Concluded. Outlet surveys at 90 percent design speed.

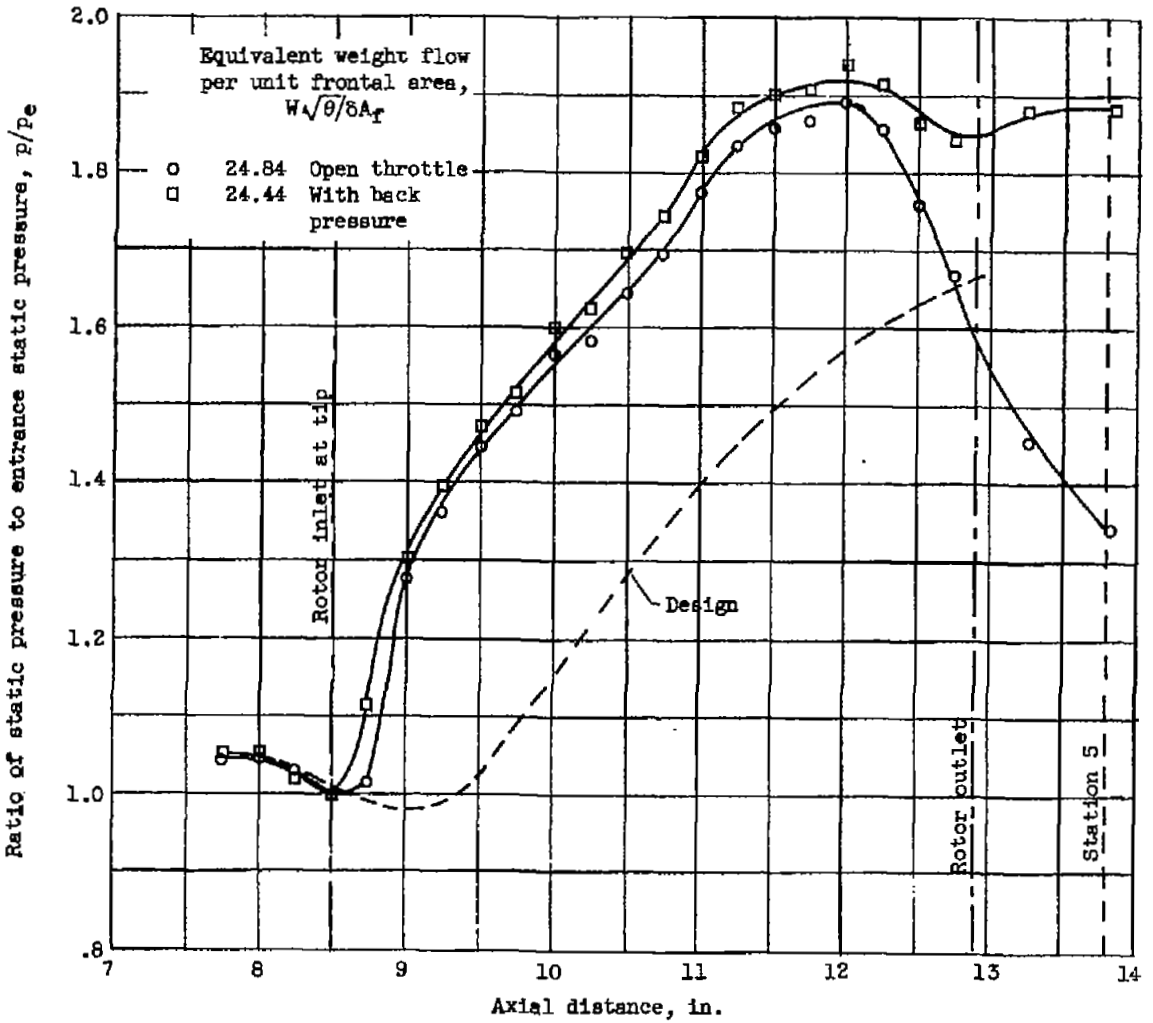

(a) Over rotor at design speed.

Figure 12. - Static-pressure profiles.

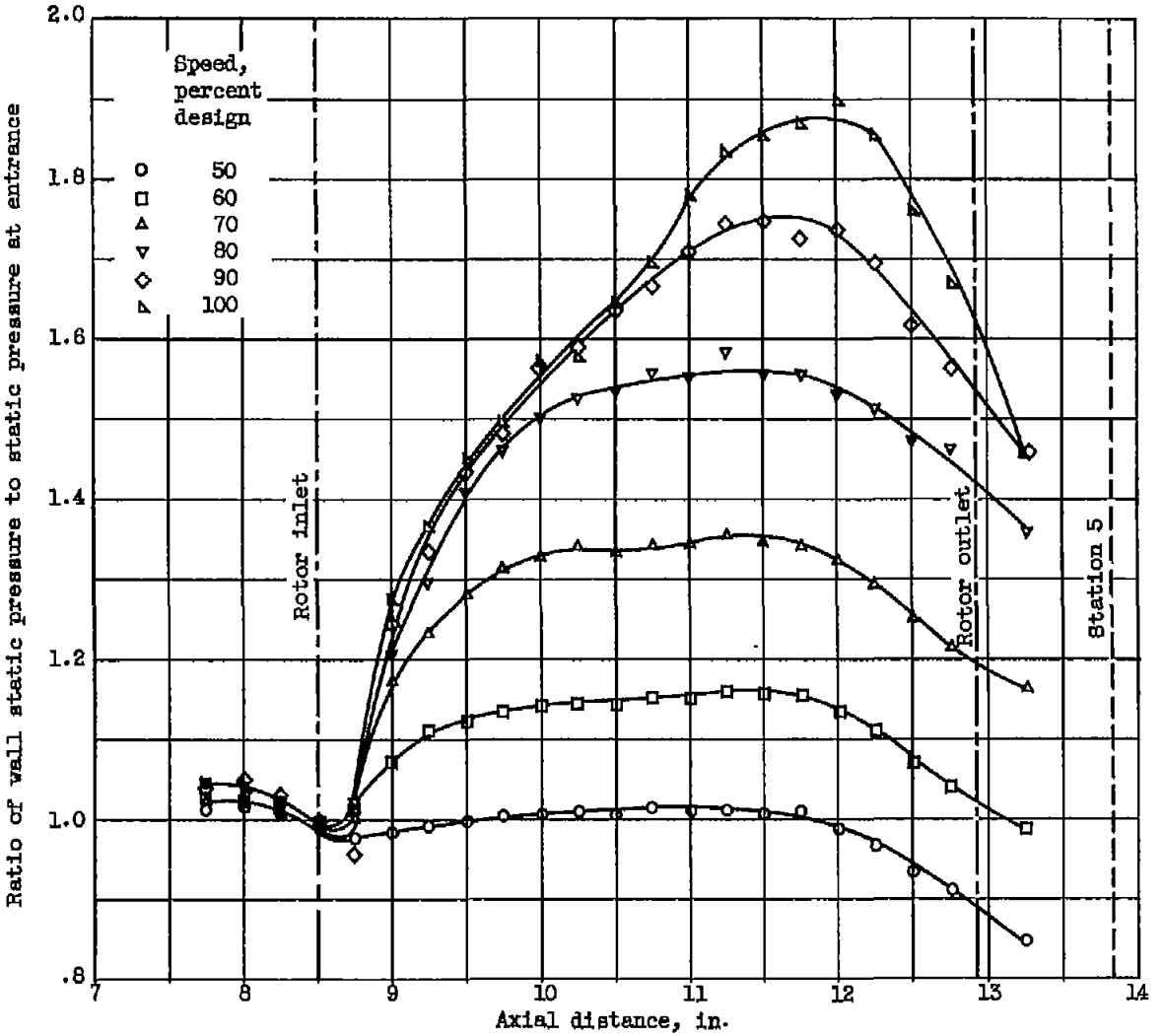

(b) At open throttle.

Figure 12. - Concluded. Static-pressure profiles.

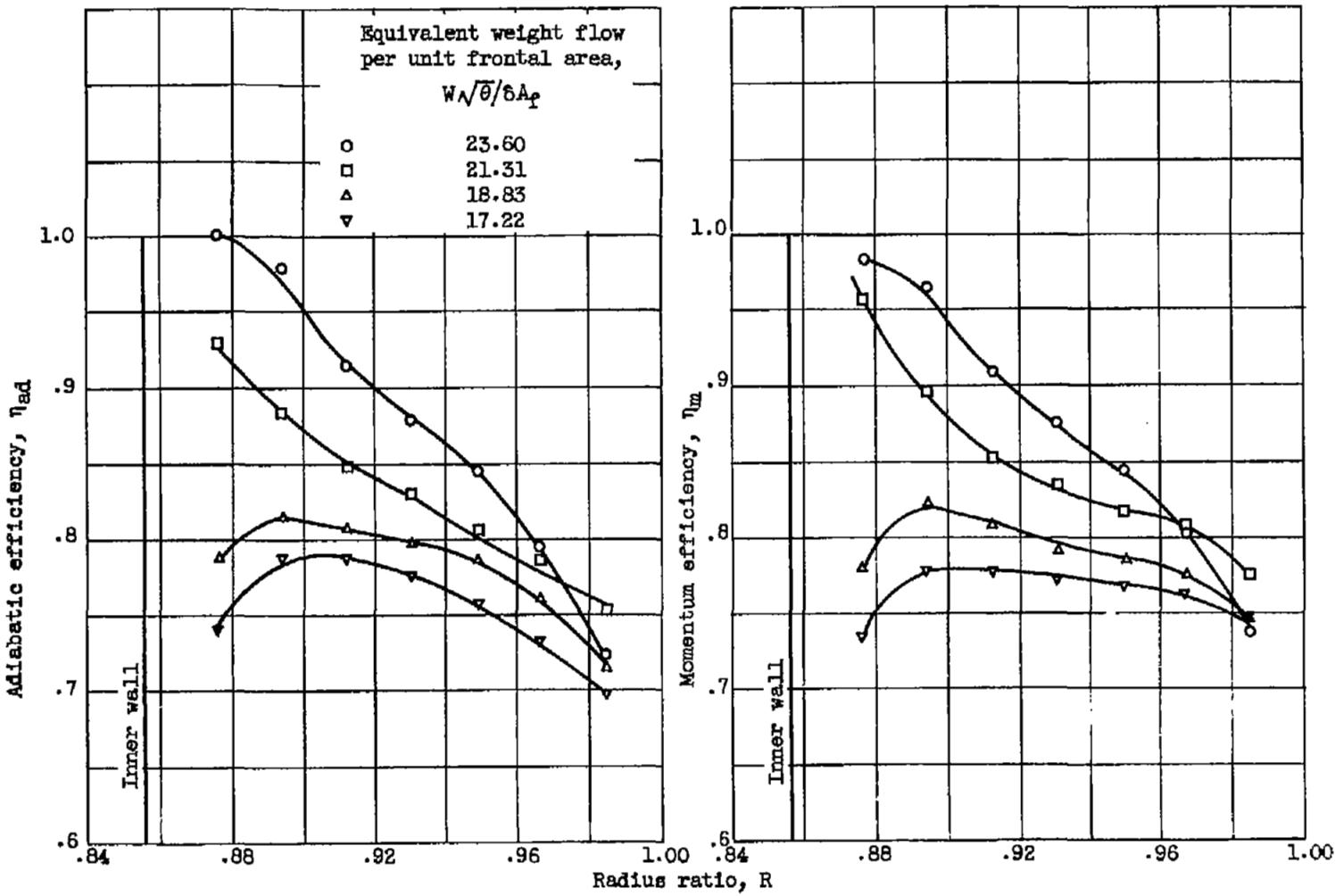

(a) Comparison of adiabatic and momentum efficiencies.

Figure 13. - Blade-element performance at 90 percent design speed.

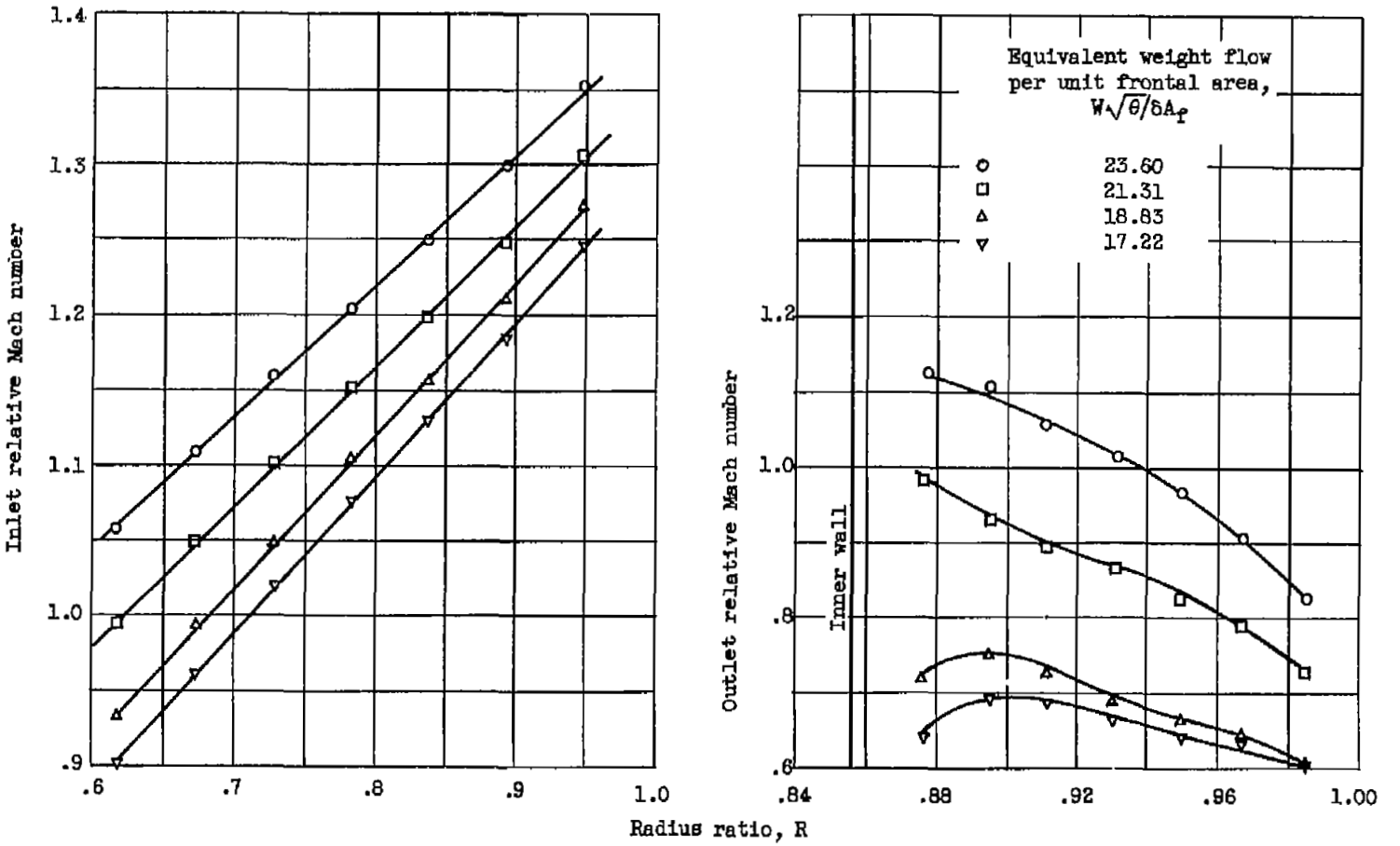

(b) Radial variation of inlet and outlet relative Mach numbers.

Figure 13. - Continued. Blade-element performance at 90 percent design speed.

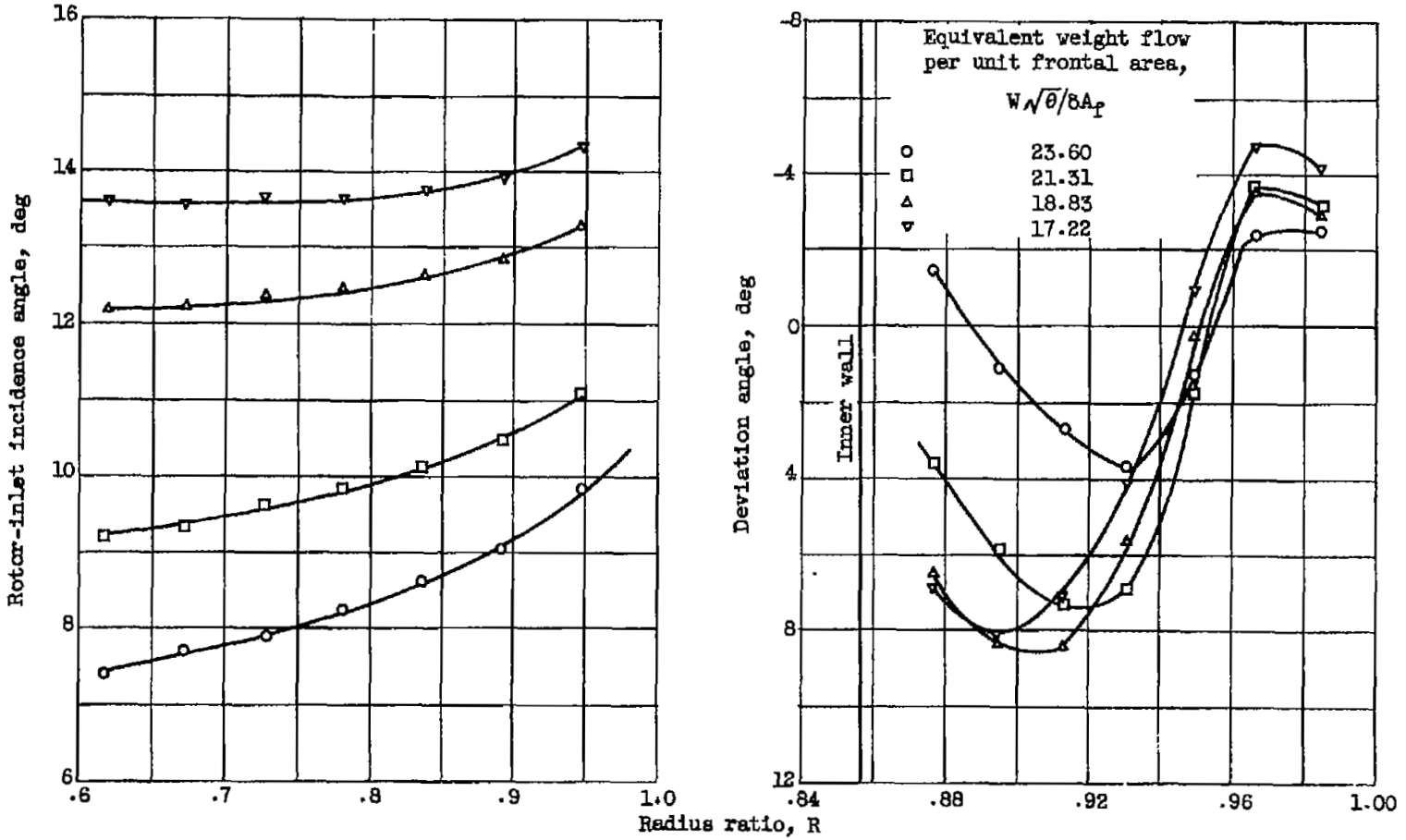

(c) Radial variation of incidence angle and deviation angle.

Figure 13. - Continued. Blade-element performance at 90 percent design speed.

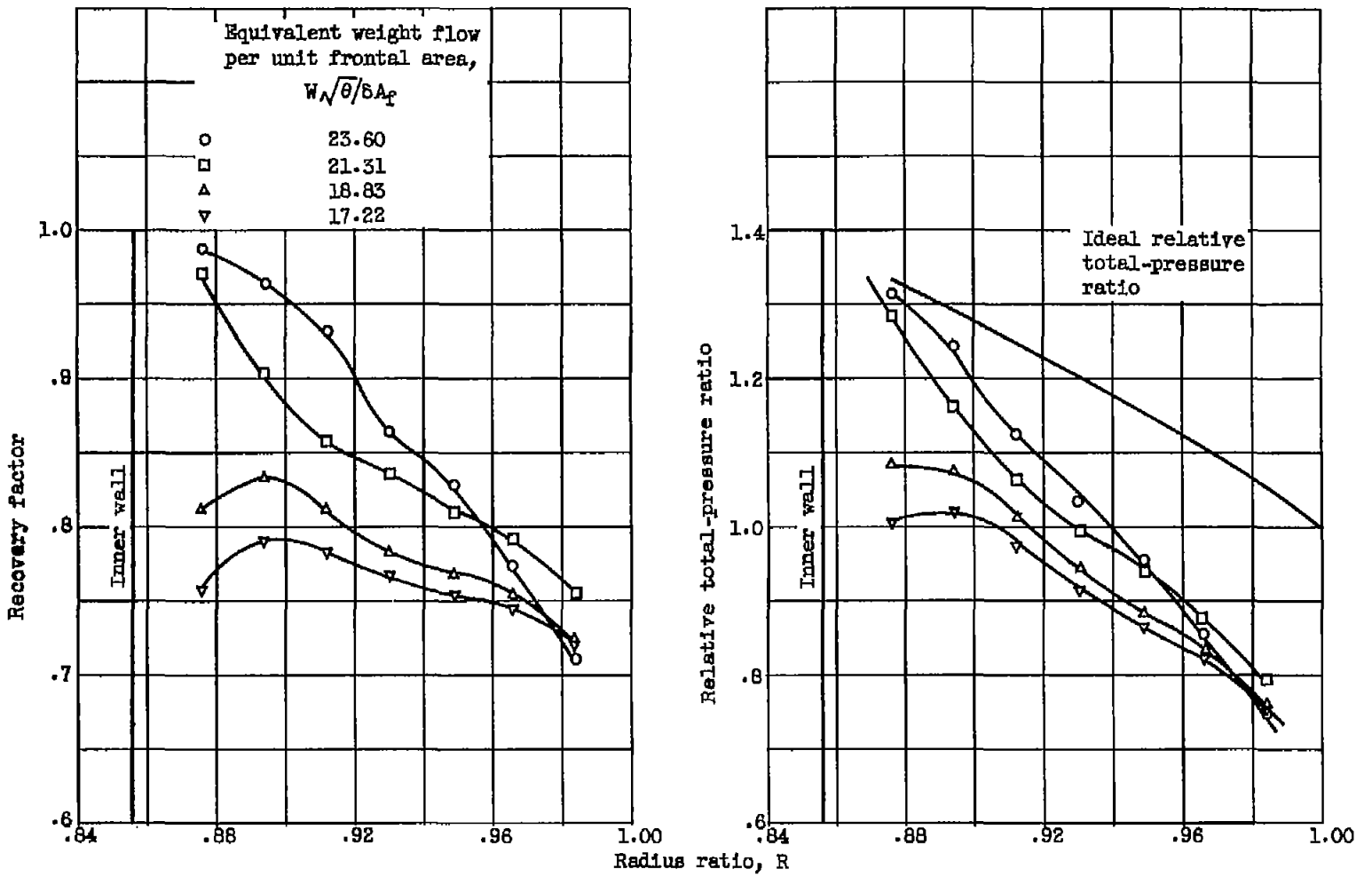

(d) Radial variation of recovery factor and relative total-pressure ratio.

Figure 13. - Concluded. Blade-element performance at 90 percent design speed.

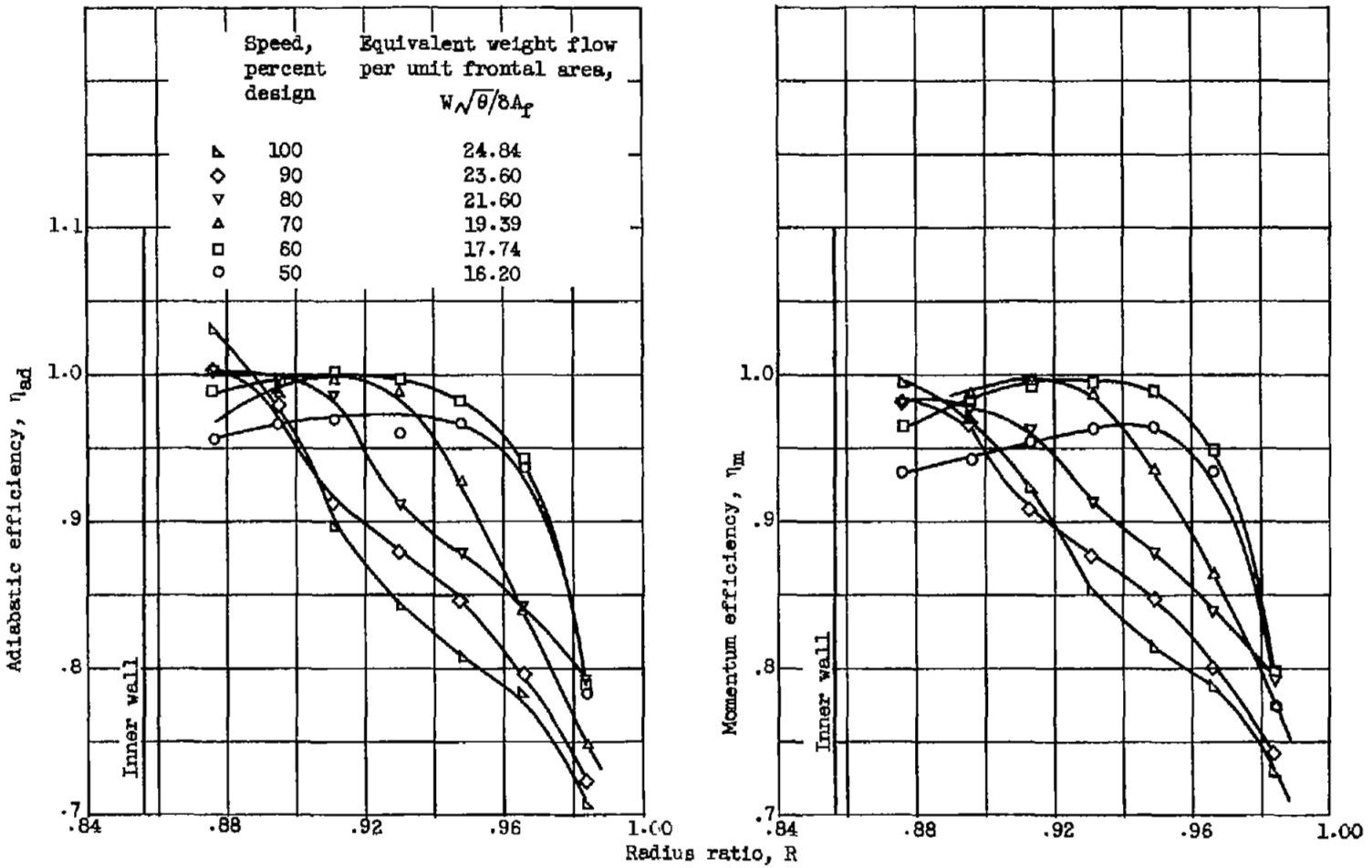

(a) Comparison of adiabatic and momentum efficiencies.

Figure 14. - Blade-element performance at open throttle.

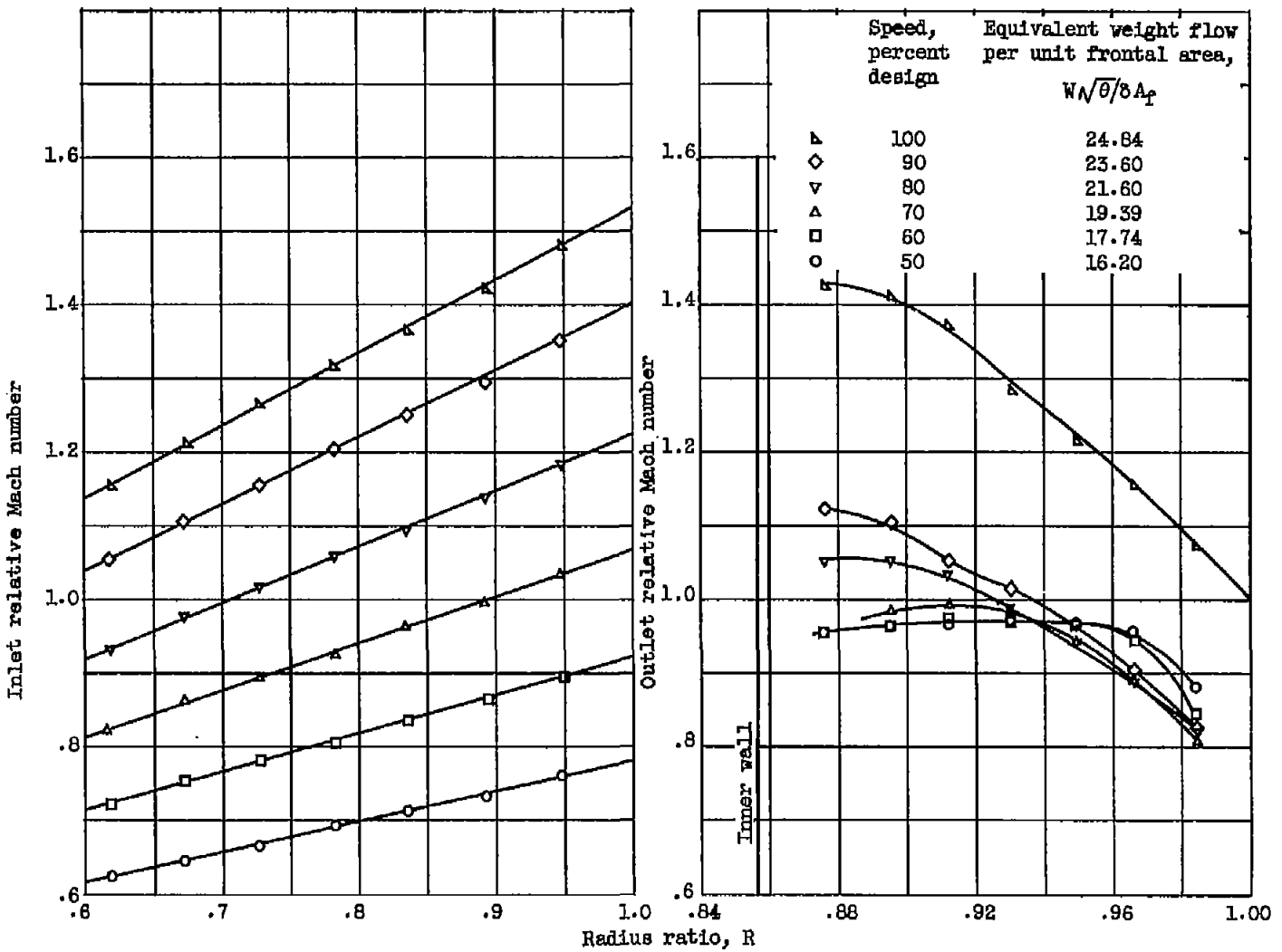

(b) Radial variation of inlet and outlet relative Mach numbers.

Figure 14. - Continued. Blade-element performance at open throttle.

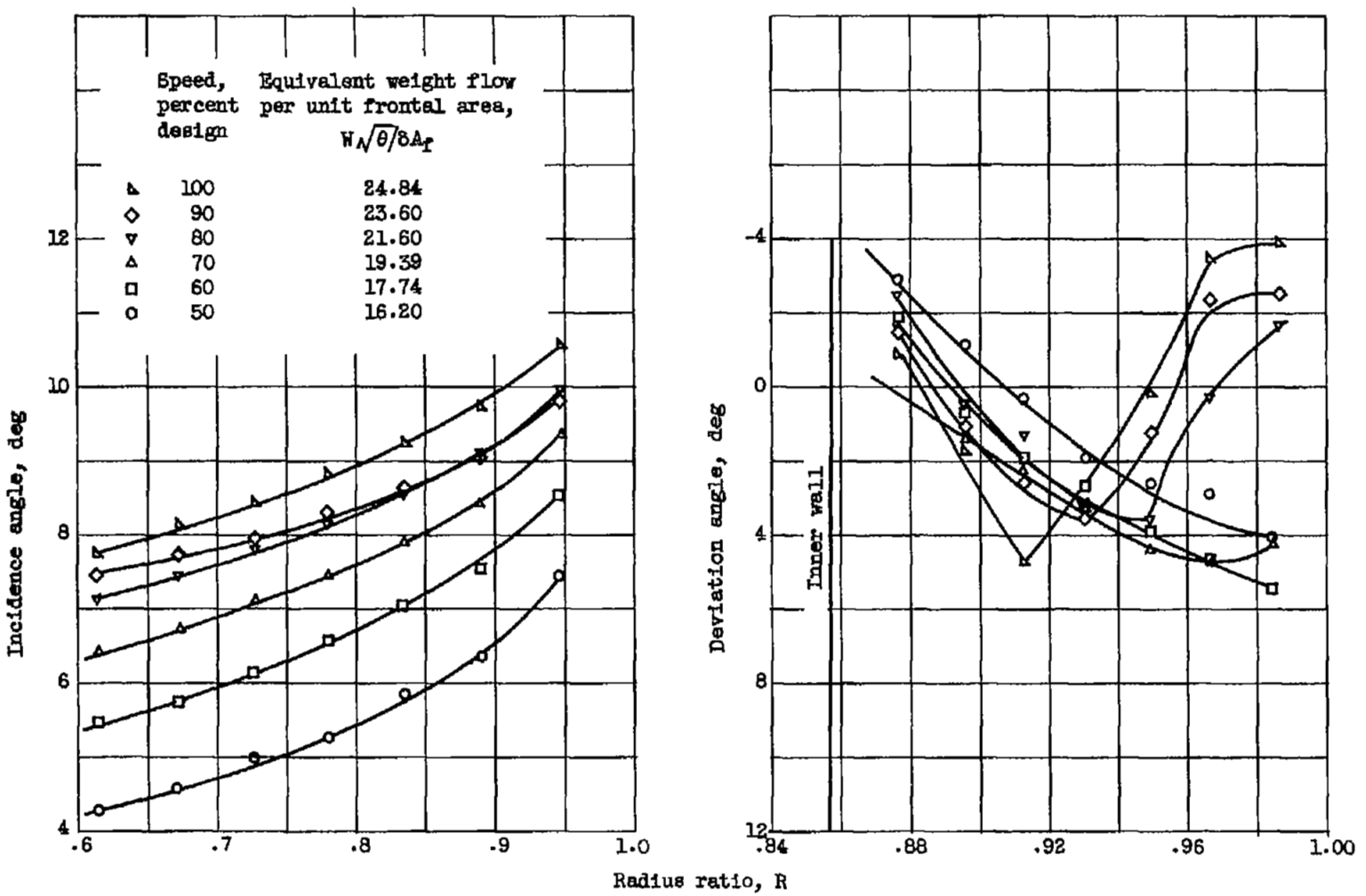

(c) Radial variation of incidence angle and deviation angle.

Figure 14. - Continued. Blade-element performance at open throttle.

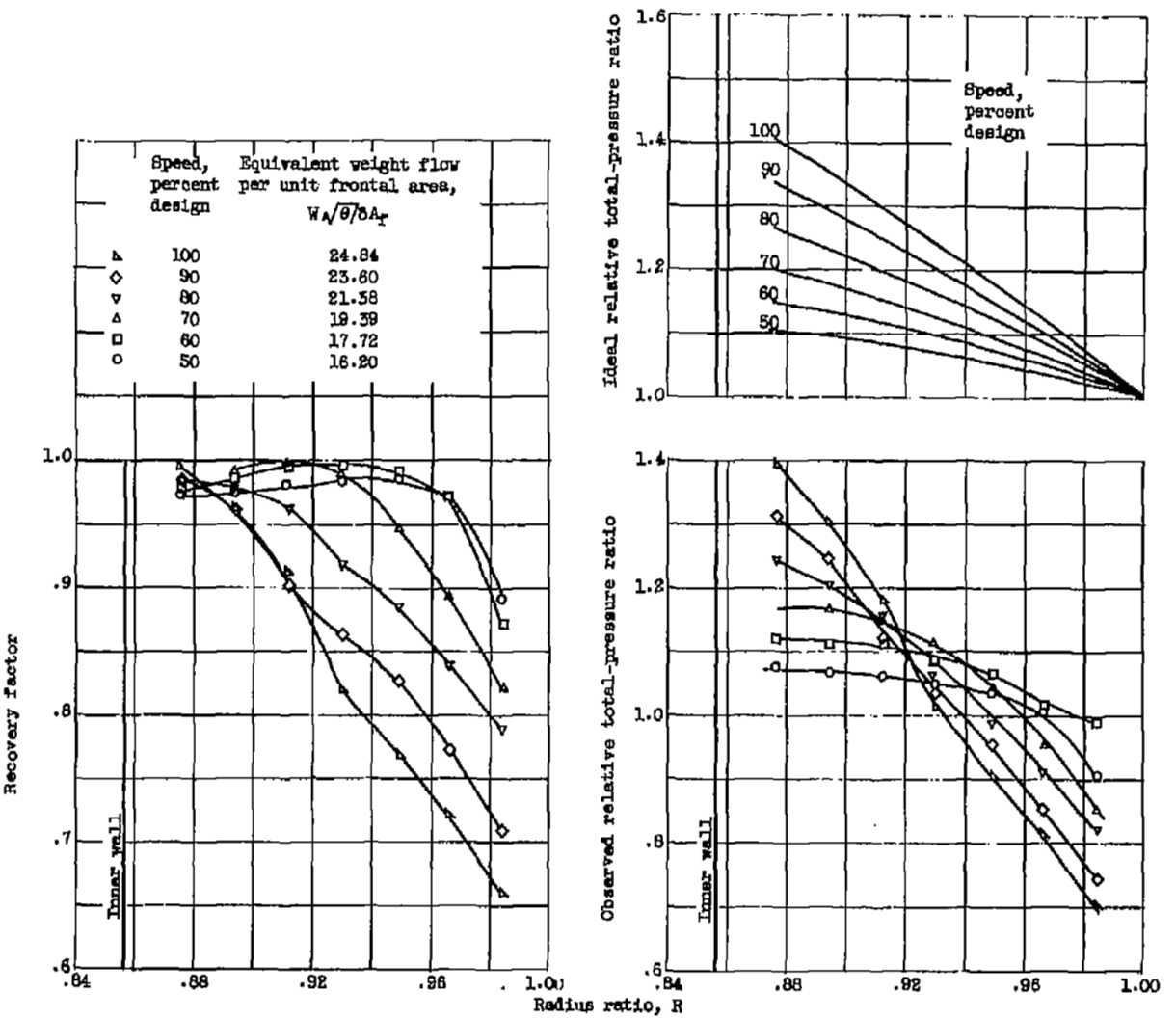

(d) Radial variation of recovery factor and relative total-pressure ratio.

Figure 14. - Concluded. Blade-element performance at open throttle.